Lenticular Galaxies - The One in The Middle

Simon Malinga

2015

A project submitted in partial fulfilment of the requirements for the degree M.Sc. in the Department of Astronomy, as part of the National Astrophysics and Space Science Programme
UNIVERSITY OF CAPE TOWN

Supervisors: Dr. Sudhanshu Barway, Dr. Kartik Sheth and Dr. Kurt van der Heyden

Abstract

The lenticular (S0) galaxies introduced by Hubble (1936) as a morphological transition class between elliptical and early-type spiral galaxies, which have the most massive bulges among disk galaxies, may have formed in several different ways as suggested by theoretical and numerical simulation studies. A sample of lenticular galaxies from the Spitzer Survey of Stellar Structure in Galaxies (S^4G) using the Spitzer Space Telescope along with Sloan Digital Sky Survey (SDSS) was used for this project to study molecular gas properties as well morphologies associated with dust where molecular gas is present. A variety of image processing techniques are employed to study the details of galaxies to uncover the presence of molecular gas in S0 galaxies. We obtained colour maps using 3.6 and 4.5 micron images and SDSS r and i band images to find these galaxies have sufficient amount of dust and molecular gas along with variety of dust morphologies. In this thesis, we have shown, for the first time that the mass of molecular gas obtained by Carbon Monoxide (CO) is correlated to colour excess measured from $(r - 3.6)$ and $(i - 4.5)$ colour maps. It would be important to study this relation using advance facilities such as ALMA and MeerKAT to explore properties of molecular gas in nearby early-type galaxies in detail.

Acknowledgements

Many people have contributed directly and indirectly, to my understanding of the content of this project. Perhaps the most important influence has been Sudhanshu Barway and Kartik Sheth, it was a great-full pleasure to work with them. I would like to thank Sudhanshu, for his guidance, hard work, research skills he taught me and other many discussions on the various astronomical topics he shared with me. Sudhanshu the journey has been an awesome one, thank you. I am also very thankful for the input of Kartik regarding my preliminary results, the comments and suggestions he provided throughout the project. Also, I would like to thank Kurt van der Heyden, Yogesh Wadadekar and Lisa Young for their useful information, comments and suggestions.

I would like to thank the National Astrophysics and Space Science Programme (NASSP) for its loyal funding throughout my four years of postgraduate studies and the National Research Foundation (NRF) facility at the South African Astronomical Observatory (SAAO) which has made the research in this thesis possible.

Also, I would like to thank my family for their strength and support. Finally, I would like to thank my colleagues and friends for technical support, comments, suggestions, moral support, and their availability when I needed them the most.

Baie Dankie al!

This research has made use the NASA/IPAC Infrared Science Archive (IRSA) and Extragalactic Database (NED), which are operated by the Jet Propulsion Laboratory, California Institute of Technology, under contract with the National Aeronautics and Space Administration. Also the Sloan Digital Sky Survey and HyperLeda database.

Plagiarism Declaration

I, Simon Malinga, know the meaning of plagiarism and declare that all of the work in the document, save for that which is properly acknowledged, is my own.

Contents

List of Figures

List of Tables

Chapter 1

Introduction

Over the past two decades, early-type galaxies were thought to be inactive and passively evolving. Recent high quality observations from ground as well as space based telescopes reveals the presence of gas, dust, star formation and stellar substructures which are challenging our understanding of the formation and evolution of these systems. A large fraction ($\sim$50$-$80%) of early-type galaxies, at least in nearby universe, are now known to possess dust features in a variety of morphological forms given that these galaxies were thought to be red and dead. A study of physical properties of dust is important to understand formation history as well as its association with molecular gas content of host galaxy.

This chapter introduces the relevant background and foundational concepts of molecular gas associated with dust in lenticular (S0) galaxies. The first section gives a general overview of the observational history and types of galaxies. The second section provides an overview of early-type galaxies in general and S0 galaxies in particular. Then followed by a discussion on molecular gas associated with dust in galaxies. Finally, the last two sections summarize the research goals and thesis outline.

1.1 General Overview

The observational discovery of galaxies began in 1755 when the German philosopher Immanuel Kant (1724-1804) noticed the fuzzy spiral objects which were visible with the small telescope. These objects were listed in catalogs of *nebulae* and clusters of stars as interesting curiosities in the sky, not to be confused with really interesting things such as comets. In 1925, Edwin Hubble (1889-1953) used the 2.54 m optical telescope on Mount Wilson Observatory to prove that the Andromeda "nebula" was actually outside of our own galaxy, the Milky Way, by using Cepheid stars for the distance measurement. He assumed that all of these stars were of the same type, with the same luminosities and concluded that the relative distances is at least 300 pc from the Milky Way. Following this work, Hubble made a number of pioneering studies of galaxies, essentially opening the field of extragalactic astronomy.

In his studies, Hubble set out a scheme for classifying the galaxies in his 1936 book, *The Realm of the Nebulae* (Hubble 1936). With later additions and modifications, he recognized four main types of galaxies: elliptical (E), lenticular (S0), and spiral (Sa and SBa), with a fourth class, the irregular, for galaxies that would not fit into any of the other categories. Elliptical galaxies range from E0 (spherical) to E7 (the most oblate). Lenticular galaxies have a bulge and smooth disk. Galaxies with the bulge and spiral arms are classified as regular spiral galaxies which are divided according to the relative size of bulge, disk and the tightness of spiral arms. Sa galaxies have the largest bulge and the most tight spiral arms, while the SBa galaxies has the large bulge and the most open spiral arms. Irregular galaxies are galaxies with only weak (Im) or no regular (IBm) structure. All of these types were revised by Kormendy & Bender (1996), and their classification scheme is well presented in Figure 1.1.

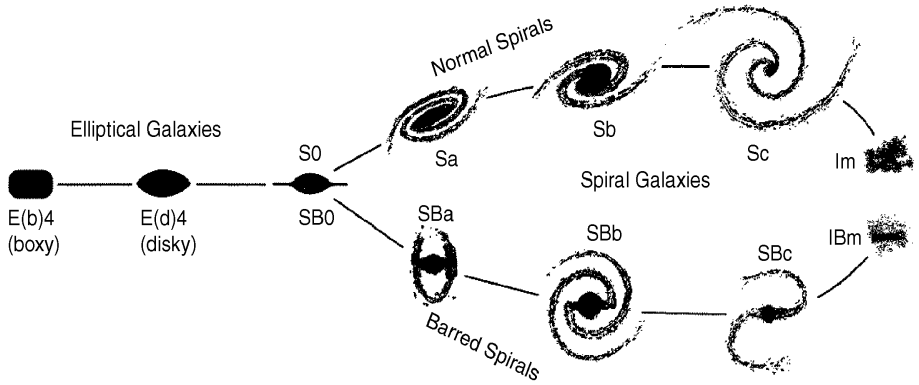

Figure 1.1: The revised Hubble classification scheme for galaxies which is well known as tuning fork diagram taken from Kormendy & Bender (1996).

In Figure 1.1, the elliptical and lenticular galaxies were denoted as "early-type" galaxies, and spirals as "late-type" galaxies. This assumed that galaxies evolved from the left (early-type ellipticals) to the right (late-type spirals) in a sequence as originally proposed by Hubble. Many modifications and refinements have been incorporated over the years, but the basic Hubble classification scheme is still widely used today.

1.2 Early-type galaxies

Early-type galaxies (ETGs) include elliptical and lenticular (S0) galaxies. Elliptical galaxies typically contain little gas and dust, no spiral arms or disk, and few hot, bright stars. Lenticular galaxies are similar to elliptical galaxies, but have a smooth disk component. These galaxies started attracting astronomer's attention with the discoveries of various physical features which were thought to be absent such as gas, dust, star formation and etc. Some of these galaxies also host active galactic nuclei (AGN), quasars and powerful radio sources.

Colour-magnitude diagram (Baldry et al. 2004) are used to divide the galaxy population in two groups; most of ETGs typically appear to lie on a 'red sequence' while spiral galaxies show bluer colours and seem to reside in a 'blue sequence' (Driver et al. 2006, Faber et al. 2007). Some of the ETGs that resides in this 'blue sequence' are star forming galaxies and of a great importance for our understanding of the formation of ETGs and the build-up of the red sequence (Schawinski et al. 2007, Salim et al. 2007, Constantin et al. 2008, Schawinski et al. 2009). These blue ETGs contain at least a few percent of young and/or intermediate-age stellar populations. One of the possible explanations of young stars in these ETGs is induced star formation as a consequence of interacting events with other galaxies in the galaxy environment. Many of simulation and theoretical studies shows that the gas-poor mergers lead to more rectangular shaped or boxy ETGs, whereas gas-rich mergers lead to disk ETGs (Naab et al. 2006).

Cappellari et al. (2011) presented ATLAS^{3D} survey of 260 nearby ETGs within 42 Mpc that provides the best constraints on dynamics and stellar populations at z = 0 through multi-wavelength studies. ATLAS^{3D} survey classified the ETGs into fast and slow rotators using their stellar kinematics. Edge-on fast rotators generally are lenticular (S0) galaxies similar to spiral galaxies with the gas and dust removed. Other fast rotators often show presence of a bar and span over the same full range of bulge fractions as spiral galaxies. The slow rotators are similar to spheroidal-like, rounder elliptical galaxies. Young et al. (2011) used the survey to study the cold gas contents, and recently, McDermid et al. (2015) used the same survey to study the star formation histories and stellar population scaling relations and found that the duration of star formation is systematically more extended in lower mass objects. Recent observations show the presence of dust, gas, star formation and stellar substructure in these galaxies (e.g., Smith et al. 2012, Crocker et al. 2011, Allen et al. 2014, Young et al. 2011, Lagos et al. 2015).

ETGs are crucial to understand the bigger picture of galaxy formation and evolution. Despite the impressive progress in the field over the past decades, further advances in the field of ETGs studies are happening due to new telescope technology and the launch of new galaxy surveys that would quantify the physical properties of these interesting objects (e.g., Cappellari et al. 2011, Kent 1994, Pota et al. 2012, Sheth et al. 2010, Côté et al. 2006).

1.2.1 Lenticular (S0) galaxies as interesting objects

The lenticular (S0) galaxies introduced by Hubble (1936) as a morphological transition class between elliptical and early-type spiral galaxies, which have the most massive bulges among disk galaxies, may have formed in several different ways as suggested by theoretical and numerical simulation studies (Bekki 1998, Abadi et al. 1999). When comparing properties, it is found that the bulges of lenticular galaxies are very similar to elliptical galaxies, while their disks have similarities to the disks of early-type spiral galaxies, except that they lack conspicuous spiral arms. Our understanding of the formation and evolution of lenticular

galaxies, in terms of the individual physical processes involved, is still unclear, in spite of extensive efforts both by observational and theoretical means.

Barway et al. (2007; 2009; 2011; 2013) have presented evidence to support the view that the formation history of S0 galaxies follows two very different routes. Which route is taken seems to depend primarily upon the luminosity of the galaxy, although the environment also plays a role. According to this view, luminous S0 galaxies are likely to have formed their stars at early epochs through major mergers or rapid collapse followed by rapid star formation, similar to the formation of elliptical galaxies (Aguerri et al. 2005). The bulges of such S0 galaxies are more likely classical bulges (Kormendy & Kennicutt 2004) sharing most of their stellar and dynamical properties with low- and medium-mass elliptical galaxies; the most massive ellipticals seem to be different (Gadotti 2009). These luminous S0 galaxies with classical bulges were studied by Hubble, and placed in close proximity to ellipticals on his tuning fork diagram. On the other hand, low-luminosity S0 galaxies likely formed by the quenching of star formation due to the stripping of gas from the bulges and disks of late-type spiral galaxies through galaxy interactions or by motion in a dense environment (Aragón-Salamanca et al. 2006, Bedregal et al. 2006, Barr et al. 2007). This fading scenario may not be applicable for the most massive (and therefore luminous) S0 galaxies harbouring populous globular clusters (Sánchez-Janssen & Aguerri 2012).

If this picture is broadly correct, there must be signatures of the formation mechanism imprinted in the various observable parameters of the galaxy. Indeed, such imprints have been seen in the surface brightness profiles (as correlated bulge disk-sizes) by Barway et al. (2007; 2009) and the presence of kinematic structures, such as a stellar bar (Barway et al. 2011, Skibba et al. 2012, van den Bergh 2012). There should also be imprints on dust and other features as traced by optical-optical and optical-IR colour maps. Available multi-wavelength data from various telescopes are very useful to determine the properties of dust and molecular gas to constrain formation scenarios in S0 galaxies.

1.3 Molecular gas

Properties of dust often dependent on the interaction of dust particles with the electromagnetic radiation, i.e., on attenuation and scattering of starlight, known as dust extinction, and re-emission by dust at longer wavelengths. Apart from the dust extinction hiding interesting astrophysical processes, it also indicate presence of various elements, such as molecular hydrogen (H_2). The molecular hydrogen content of early-type galaxies can be characterized with many different techniques but they are generally rely on two effects, that is, absorption of stellar light or the re-emission of the absorbed energy at the infrared and sub-millimeter wavelengths.

Most of the previous molecular hydrogen studies of early-type galaxies focus on the re-emission of the absorbed energy at sub-millimeter wavelengths of molecule hydrogen using Carbon Monoxide (CO; e.g., Davis et al. 2015, Alatalo et al. 2015, Li et al. 1993, Liszt 2007, Young et al. 2011, Sadler 1985, Bohlin et al. 1978, Sheth et al. 2002, Allen et al. 2014). These studies derived the total H_2 masses from the CO fluxes by listing a fixed conversion ratio as $X = N_{H_2}/I_{CO} = M_{H_2}/L_{CO}$. The most often quoted value of conversion ratio is $X = 3 \times 10^{20}$ cm^{-2} ((K km s^{-1})$^{-1}$; Liszt 2007, Liszt et al. 2010). Young et al. (2011) have shown that this value of the conversion ratio leads to H_2 masses in solar units given by $M_{H_2} = 6.0 \times 10^4 D^2 I_{CO}$, where D is the distance in Mpc and I_{CO} is the integrated intensity to an H_2 column density averaged over the beam in (K km s^{-1})$^{-1}$. As it should be indicated, the conversational ratio is significantly different from one galaxy to another and this has been strongly proven by several observations (Solomon et al. 1997, Liszt 2007). There are in fact physical phenomena that can account for variation of this ratio (e.g., temperature, density and chemical composition; Guélin et al. 1993, Wilson et al. 1995, Neininger et al. 1996). For example, the observational evidence showing a strong increase either due metallicity or excitation problems (Guélin et al. 1993, Neininger et al. 1996, Israel 2000). Another example is the one of the Magellanic Clouds, where the conversion ratio X might be 10 times higher than the standard ratio (Solomon et al. 1987, Rubio et al. 1993). Therefore, the apparent molecular gas mass derived using the conventional ratio may have little to do with the real molecular gas mass, and really reflects only the CO luminosity (see Figure 1.2).

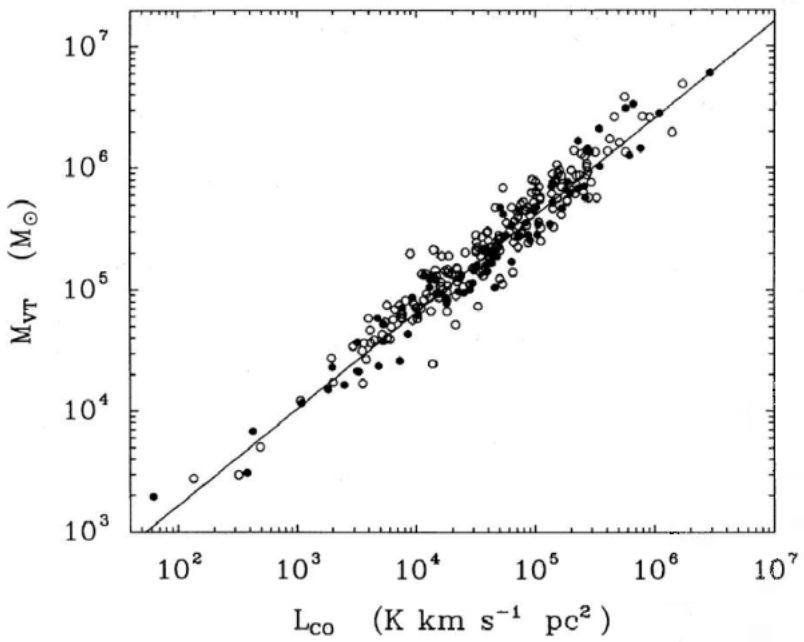

Figure 1.2: The virial mass against the CO luminosity for molecular clouds in the Milky Way, where the fit from Solomon et al. (1987) data corresponds to $M_{VT} \propto {L_{CO}}^{0.76}$.

The presence of H_2 molecule is mostly inferred essentially from the CO emission, but another important component is mapping the H_2 molecules directly using broad-band imaging from dust emission where the Rayleigh-Jeans domain of thermal emission is dominated by the near-infrared (near-IR) continuum from warm dust (Allamandola et al. 1999). This continuum was previously known as the unidentified infrared bands features centered at the infrared and are currently attributed to polycyclic aromatic hydrocarbons (PAHs), a label of organic compounds containing only carbon and hydrogen that are composed of multiple aromatic rings, which can be described well by the concept of the spectral energy distribution (SED) of star formation in galaxies.

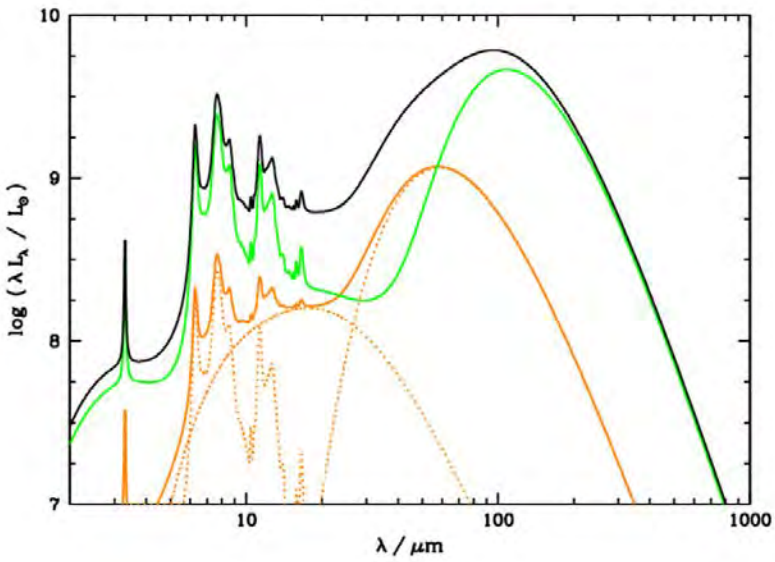

Figure 1.3: The SED model of a typical young stellar objects associated with dust emission of a simulated galaxy from the da Cunha et al. (2008) model (black curve) demonstrating the individual contributions from the birth cloud dust (orange) and hot dust (green).

Figure 1.3 shows the SED of a typical young stellar objects associated with dust clouds that are denser and colder than the diffuse interstellar medium (ISM), showing the attenuation of UV/optical starlight by dust, and re-emission of the energy at infrared wavelengths. The emission at $\lambda \geq 20$ μm is dominated by two thermal components at different temperatures, one of which represents warm dust surrounding the molecular gas clouds from which stars and star clusters form. The emission from a cold component at $T \sim 20 - 30$ K becomes increasingly dominant at longer wavelengths. This cold dust exists in the diffuse clouds, warm dust can dominate the bolometric luminosity in a high star formation rate in galaxies. The cold dust has been shown to contain most of the dust mass in many galaxies.

1.4 Research Motivations and Goals

The early-type galaxies were not known to have gas and dust. This view has changed by recent observations which reveals the presence of dust and gas in these galaxies (e.g., Smith et al. 2012, Crocker et al. 2011, Allen et al. 2014, Young et al. 2011, Lagos et al. 2015). The gas in these galaxies contains atomic and molecular hydrogen, where both components in dusty-regions are caused by the chemical reaction occurring on surfaces of interstellar grains resulting in typically extinction related to the column of hydrogen, $N(H_{tot}) = 1.9 \times 10^{21}$ A_V cm^{-2}. mag^{-1} (Binney & Merrifield 1998, Pirronello et al. 2004). This relation seems to hold to first order whether the gas is atomic or molecular, and can be justified analytically if the grain properties are assumed to be universal so that the extinction curve is the same for all lines of sight. However, even in the Milky Way, there appears to be a difference in the dust grain properties between interstellar clouds that have and have not undergone shocks. Shock heating of the grains in faster moving clouds is assumed to change the properties of the grains.

These considerations motivate our study of molecular gas using a typical dust extinction measured by dividing one broad-band image in a given colour by another. The amount of extinction varies with wavelength. The molecules are able to scatter light because the electromagnetic field of the light waves induces electric dipole moments in the molecules, thus the interstellar extinction curve is well studied and therefore by comparing two images at different wavelengths we can, in principle, quantify the effects of dust. The traditional broad-band images from the shortest wavelengths in the optical (r and i) to the longest wavelengths in the near-IR (3.6 and 4.5 μm) are useful for this purpose. Thus the dust extinction is measured using any combination of these filters but one can broadly divide the resulting colours into optical-IR colours (e.g., r-3.6, i-4.5) and infrared-infrared colours (e.g., 3.6-4.5). Of these various combinations, the colour map produced with the optical-IR colour (for example r-3.6) is known to show presence of molecular gas detected using CO observations of nearby galaxies (Sheth et al. 1998).

In this thesis, we study the molecular gas presence by examining dust extinction in lenticular (S0) galaxies in the nearby universe using with the colour map technique describe in the previous paragraph. We present our near-IR (3.6-4.5) colour maps based on Spitzer Survey of Stellar Structure in Galaxies (S^4G; Sheth et al. 2010) as well as optical-IR (r-3.6, i-4.5) colour maps from Sloan Digital Sky Survey (SDSS) and S^4G data. These colour maps are analyzed to determine dust morphologies as well as to derive near-IR colour-excess. For the first time, we show that near-IR colour-excess is correlated with mass of molecular gas measured using CO observations.

1.5 Thesis outline

The thesis is organized as follows:

[1] The current Chapter introduces the context and motivation for this research. This Chapter is divided into five parts; The General overview, Early-type galaxies along with S0s as interesting objects, Molecular gas, the research motivation and goals, and the last section is the thesis outline.

[2] Chapter 2 discusses the sample and its selection from Spitzer Survey of Stellar Structure in Galaxies (S^4G) and Sloan Digital Sky Survey (SDSS).

[3] In Chapter 3, we describe in detail the method used to determine the colour maps. We also present analysis of dust morphologies in S0 galaxies.

[4] The results are presented in Chapter 4, where we compare optical-IR colour-excess with the existing CO masses of molecular gas observations from the literature.

[5] The last Chapter reviews and summarize the work done, also it explore the future possibilities of the current work.

Chapter 2

Data

This chapter describe an overview of the Spitzer Survey of Stellar Structures in Galaxies (S^4G) survey with brief information on the Spitzer Space Telescope and the Infrared Array Camera (IRAC) which were used in this survey. We also describe Sloan Digital Sky Survey (SDSS) survey. Finally, we give details of our sample and data used for this work.

2.1 The Spitzer Survey of Stellar Structures in Galaxies

The Spitzer Survey of Stellar Structures in Galaxies (S^4G) is a volume-, magnitude-, and size-limited survey of ∼2300 nearby galaxies at 3.6 and 4.5 μm that provide an ultimate baseline data set to study stellar mass and stellar structure in nearby galaxies (Sheth et al. 2010). Data were acquired between 2010 and 2012 with the 85 cm Spitzer Space Telescope and Infrared Array Camera (IRAC; Fazio et al. 2004) in 3.6 and 4.5 μm channels to reduce dust extinction and contamination from star formation that are quite difficult to conduct from the ground. The goals of the survey were to obtain a detailed understanding of the properties of the different stellar structures, their formation and evolutionary paths, and their role in the broader picture of galaxy evolution using an extremely deep survey reaching an unprecedented 1σ surface brightness limit of $\mu_{3.6\mu m(AB)} = 27$ mag.arcsec^{-2}.

S^4G survey consist of the sample galaxies with radial velocity of $V_{sys,\ radio} < 300$ km.s^{-1}, corresponding to a distance of $d < 40$ Mpc for a Hubble constant that is about $H_0 = 75$ km.s^{-1}.Mpc^{-1}, total of corrected magnitude of $m_{B_{corr}} < 15.5$, and blue light isophotal angular diameter of $D_{25} > 1.0'$ at Galactic latitude of $\mid b \mid > 30°$ are chosen using HyperLeda database (Paturel et al. 2003). The exposure time for each galaxy was 240 s and were then mapped between 1 and $1.5 \times D_{25}$. The root mean square noise (σ) level of 0.0093 and 0.0072 MJy.sr^{-1} at 3.6 and 4.5 μm, respectively. The survey maps galaxies to its faintest stellar densities in its outskirts, where the azimuthally averaged surface brightness is measured to $\ll 1$ M$_\odot$pc^{-2} and this makes it ideal for the study of mass distribution as well as stellar structures in galaxies.

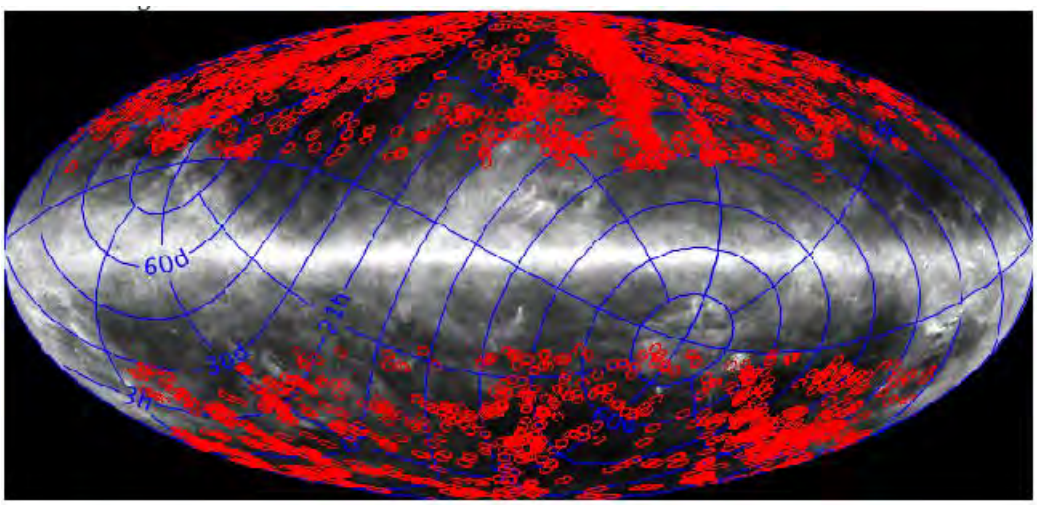

Figure 2.1: The galaxies from S^{4}G are plotted on top of the zodiacal background with the IR background (Sheth et al. 2010, Infrared Science Archive (IRSA[1])).

The volume of 40 Mpc is chosen to be large in order to have nearby galaxies of all types and to be representative of a large range of the local large-scale structure environment. The local large-scale in Figure 2.1 is the distribution of S^{4}G galaxies as a function of Hubble type and stellar mass galaxies in red circles.

S^{4}G data was observed by the National Aeronautics and Space Administration (NASA) space-based infrared telescope, Spitzer Space Telescope. This telescope was an improvement of Infrared Astronomical Satellite (IRAS). Spitzer has an 85 cm diameter telescope mirror, and three scientific instruments providing imaging and spectroscopy at wavelengths from 3.6 to 160 μm (Gehrz et al. 2007). For imaging, Spitzer is using Infrared Array Camera (IRAC) and Multi-band Imaging Photometer for Spitzer (MIPS; Rieke et al. 2004), and for spectroscopy it uses the low and high resolution of Infrared Spectrograph (IRS; Houck et al. 2004). All of these instruments are using different wavelengths, and Table 2.1 present the exact wavelength channels of Spitzer scientific instruments. The current details on Spitzer status and performance can be found on the Spitzer Science Center website[2].

Table 2.1: The exact wavelength channels of Spitzer scientific instruments.

Instrument	Wavelength channel
IRAC	3.6, 4.5, 5.8 and 8 μm
MIPS	24.0, 70.0 and 160.0 μm
IRS	5.3-14.0 and 14.0-40.0 μm for low resolution
	10.0-19.5 and 19.0-37.0 μm for high resolution

[1] At `http://irsa.ipac.caltech.edu/data/SPITZER/S4G/`
[2] At `http://ssc.spitzer.caltech.edu`

During Spitzer cryogenic mission 597 of S^{4}G 2331 galaxies were observed; 125 of these are part of the LVL survey, and 56 are from the SINGS survey, both of which used the same strategy that was deploy for S^{4}G. A total of 1734 galaxies were observed as a part of S^{4}G survey during post-cryogenic mission, and were mapped using either a small dithered map or a mosaicked observation for both IRAC channels' on-source with an integration time of 240 s. This led to the root mean square noise of $\mu(1\sigma) \sim 0.0072$ and 0.0093 MJy.sr^{-1} at 3.6 and 4.5 μm, respectively.

For the new observations, 1560 are galaxies with $D_{25} < 3.3'$. These galaxies are mapped to $1.5 \times D_{25}$ by using a single pointing, because the Spitzer field of view is $5'$. All of these galaxies are mapped using a standard-cycling small dither pattern with four exposures of 30 s each in two separate Astronomical Observation Requests (AORs). In order to allow a sufficient rotation of the telescope, each pair of AORs is separated by at least 30 days of which the galaxy is imaged at two distinct orientations. Two AORs is used to remove of cosmic rays, and the redundant information gathered by the two visits characterize and remove image artifacts. The data drizzling from the two visits is meant to achieve the sub-pixel sampling with which reconstruct images with better fidelity that would be possible from a single visit. Since IRAC channels collect data simultaneously, their offset placement in the Spitzer focal plane is added on the flanking map in order to adjacent to the galaxy in each of the two channels. The left panel of Figure 2.2 show an example of AORs of this observations.

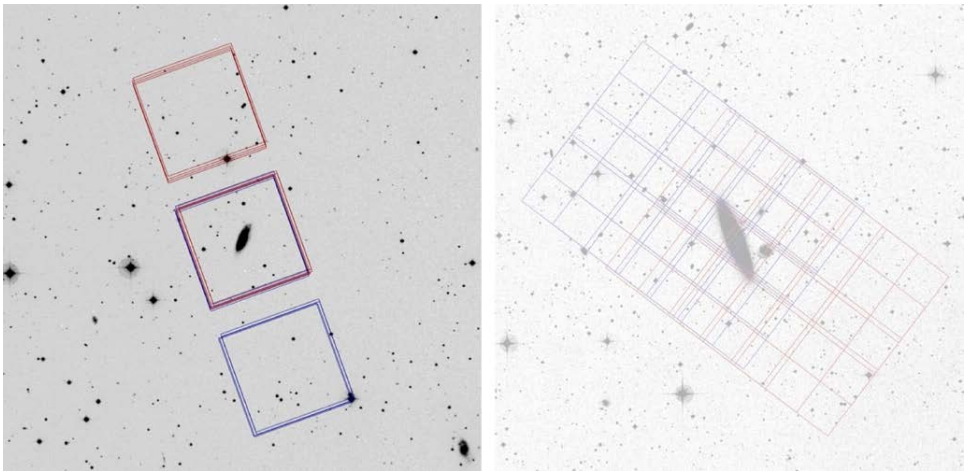

Figure 2.2: The left panel is a typical dithering AOR shown for NGC 2919 in the warm mission. On the right panel is a typical mosaicking AOR shown for NGC 1515 in the warm mission. The blue (red) grid show the coverage of the 3.6 μm (4.5 μm) IRAC channel. These channels map a galaxy to $\geq 1.5 \times D_{25}$ (Sheth et al. 2010).

For all galaxies that were observed at $D_{25} \geq 3.3'$, their array coordinates are mosaic with offsets of 146.6″ with 30 s integrations at each location to create a map $\geq 1.5 \times D_{25}$. This led to mapping of each pixel observed four times at all wavelengths in the core of the map. In addition, on each side of the galaxy there will be a region where each pixel is observed twice, but only in one of the two channels. Like the dithered AORs, each mosaic is observed twice, but with only a follow-on constraint so that each mosaic overlaps the other closely. The right panel of Figure 2.2 show an example of AORs of this observations.

The S^4G data reduction strategy was divided into four parts, which are referred as Pipelines 1, 2, 3 and 4. All of these pipelines have different objectives. For this work, we use Pipeline 1 (P1) which takes the raw basic calibrated data fits images from the two visits of each target and converts them to science-ready data. P1 start with matching the background levels in the individual images in order to find the regions of overlap between all pairs of overlapping images, and reduce the number of pixels from 20 0000 to 5000. In this process the point-spread function (PSF) is estimated by combining stars in the foreground and background regions for six typical S^4G galaxies to create a better PSF, which has a typical Full Width at Half Maximum (FWHM) of 1.7″ and 1.6″ at 3.6 and 4.5 μm, respectively. Within the regions the brightness level of 20% pixel is determined in order to avoid detector artifacts, which can affect the median. This also improve the chances of using the true sky level. Then a least-squares solution using the brightness differences between all the pairs of overlapping images is performed, the purpose of this step is to minimize the residual background difference. The background level of the first image is set to zero point due to the use of the difference of the images. After setting the first images to zero point, then they are corrected by adding the solved for corrections and used in the formation of the final mosaic. The final mosaic is created by following the standard prescription of the Space Telescope Science Data Analysis System (STSDAS) dither package. This method removes the cosmic rays by first forming a mosaic from a median combination of the images and then comparing the individual images with the median mosaic and flagging any cosmic rays. The final mosaic is formed by drizzling the individual images and it has a pixel scale of 0.75″ which was corrected to keep the units of MJy.sr^{-1}. Thus, the data can be used for different science purposes, but this depends to the goal of the research. Sheth et al. (2010) give more details for other pipelines after the data reduction of the survey.

2.2 Sloan Digital Sky Survey

Sloan Digital Sky Survey (SDSS; York et al. 2000) is an optical imaging and spectroscopy survey that provide the data for study of galaxies, quasars and stars. The SDSS survey has more than 12 data releases, and all of their data is available for the public access. The goal of the SDSS was to provide the data to support detailed investigations of the distribution of luminous and non-luminous matter in the Universe.

The survey uses a dedicated 2.5 m wide-angle optical telescope located at Apache Point Observatory near Sacramento Peak in Southern New Mexico. This telescope has two sets of charge-coupled device (CCD) arrays, one for five optical bands and the other for two digital spectrograph's to obtain the spectra. The five optical bands array consist of 30 2048 $\times$ 2048 of Tektronix CCDs that are placed in an array of six columns and five rows, and each row of an array observe the sky through a different filter u, g, r, i and z with the exact wavelengths limits of 0.36, 0.47, 0.62, 75 and 0.89 μm, respectively. The pixels have a size of 0.396$''$ on the sky with the five filters sweeping the sky as the detector covers the sky in great circles at the sidereal rate; the effective exposure time per filter is 54.1 s, and 18.75 deg^2 are imaged per hour in each of the five filters. The images have a series of pipelines producing the data that has been calibrated with astrometry, and brightnesses, positions, and shapes of objects are also determined on this process. The photometry is calibrated to an AB system magnitude, and the zero points of the system are known to 1-2%. There are two ways of calibrating the photometry, one being tying to photometric standard stars measured by a separate 0.5 m telescope on the site, and the second is an ubercalibration process by Padmanabhan et al. (2008). This process is using the overlap between adjacent imaging to tie the photometry of all the imaging observations together. The results of this processes are available in the data release. The second set of the telescope are the photometric catalogs of spectroscopy, which we don't cover in this work.

The optical data used in this work was collected from Knapen et al. (2014) data release, whereby they selected 1252 galaxies in S^{4}G sample that had imaging in SDSS. From this data we selected S0 galaxies that show dust. In Figure 2.3, we present the colour images of SDSS S0 galaxies for our sample.

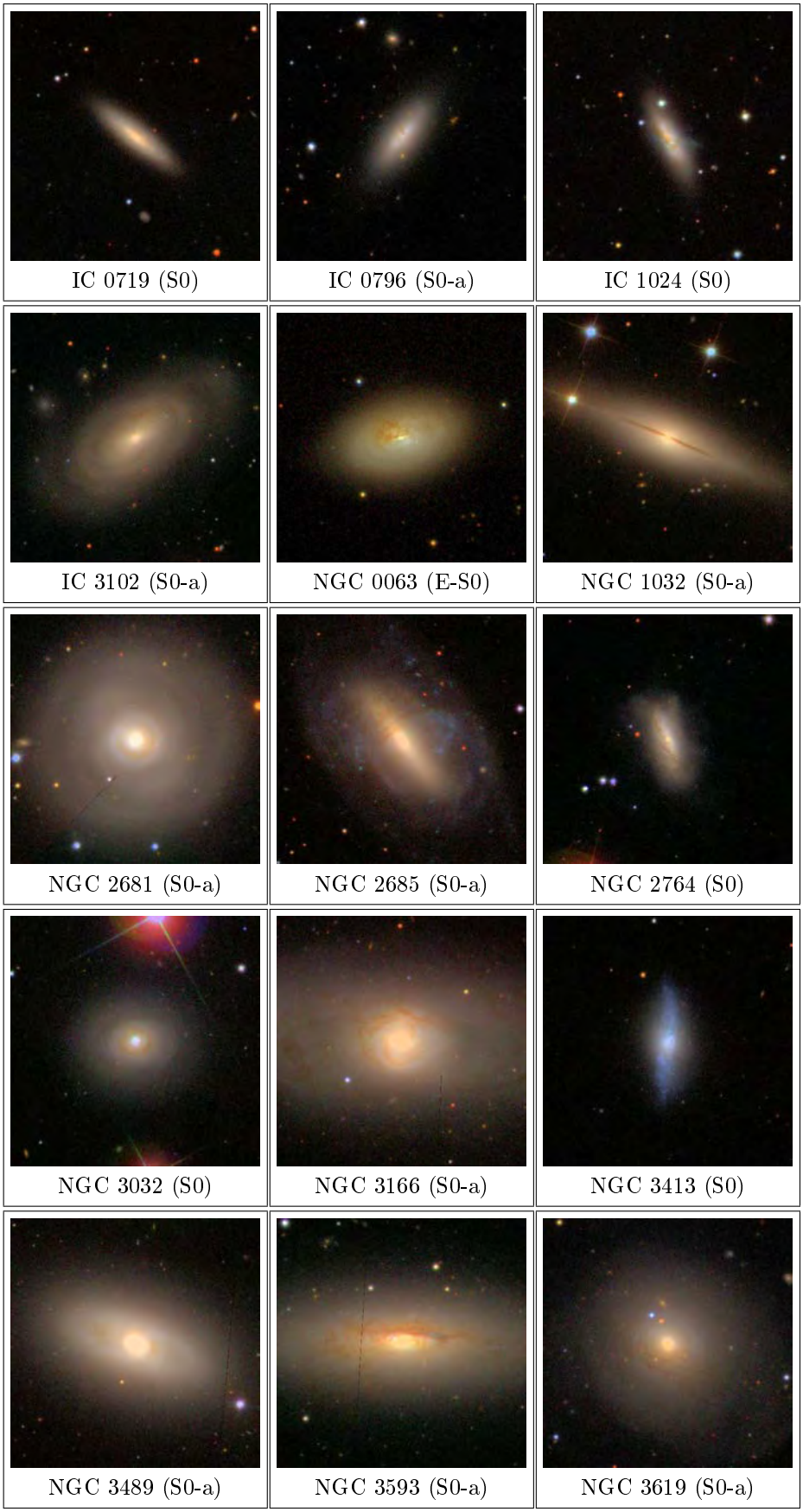

Figure 2.3: The SDSS colour images of S0 galaxies, with scales on the sky of 512×512 pixels. The red colour indicate dust region. In these images the North is up and East is to the left.

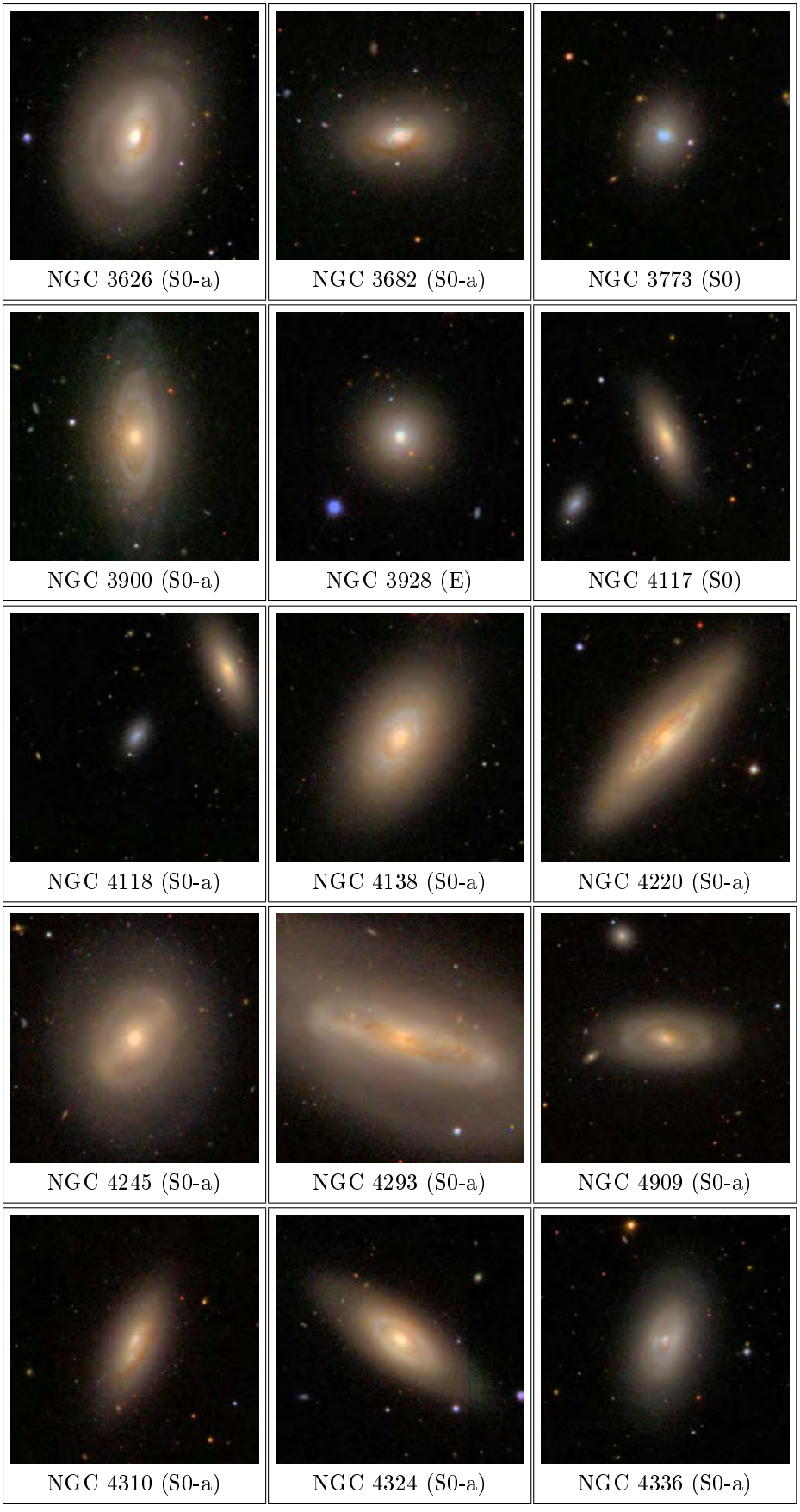

Figure 2.3: *Continued*

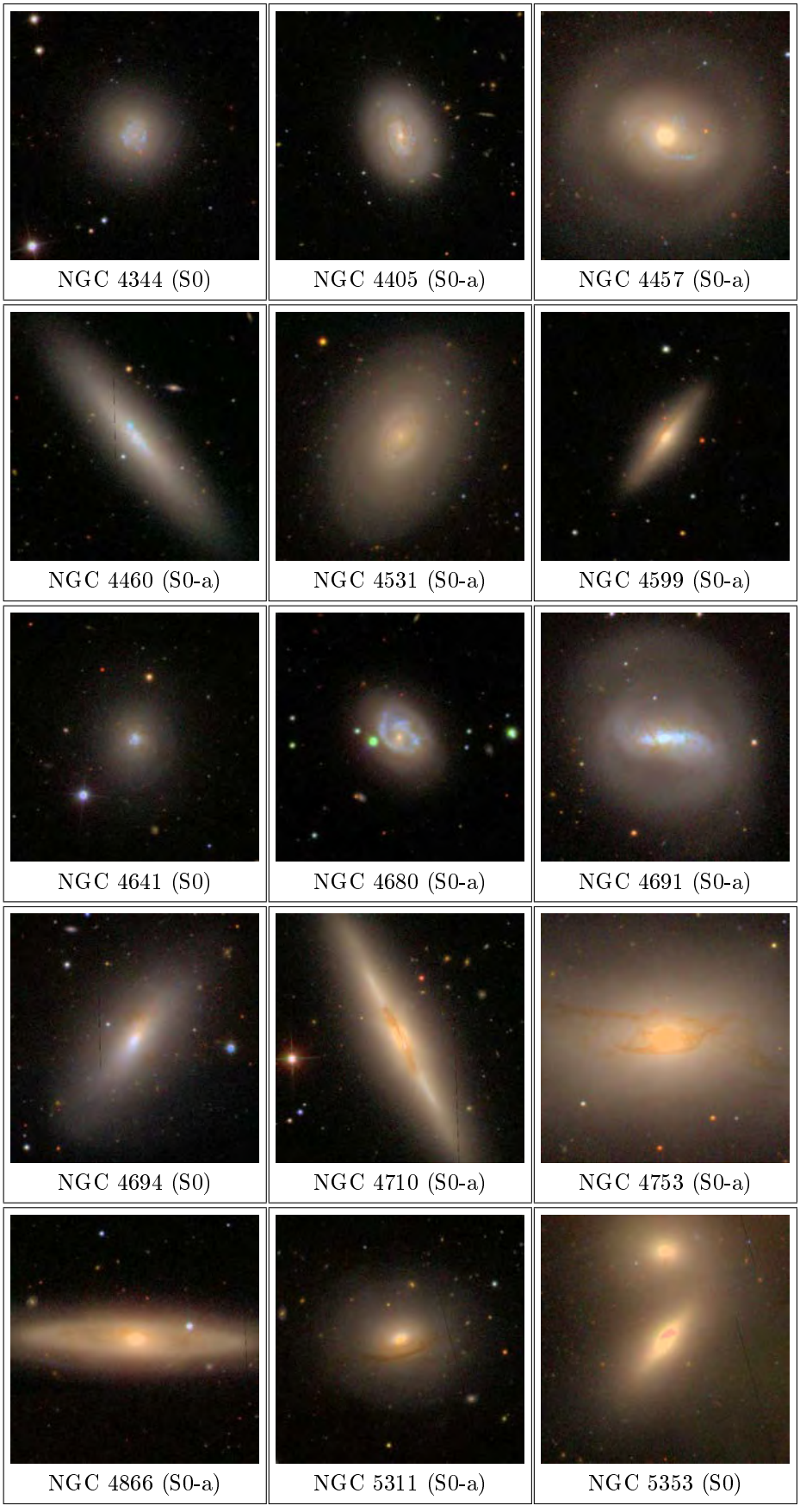

Figure 2.3: *Continued*


NGC 5354 (S0)


NGC 5360 (S0-a)


NGC 5363 (S0-a)


NGC 5422 (S0-a)


NGC 5587 (S0-a)


NGC 5631 (S0)


NGC 5689 (S0-a)


NGC 5750 (S0-a)


NGC 5953 (S0-a)


NGC 6014 (S0)


NGC 7564 (S0)

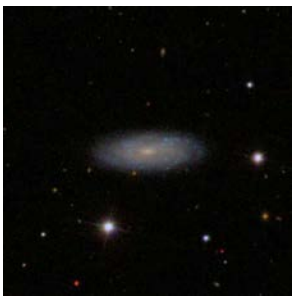
UGC 05695 (S0-a)

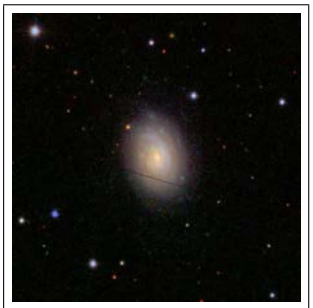
UGC 10803 (S0-a)

Figure 2.3: *Continued*

2.3 Sample

The sample investigated for this work was primarily drawn from S^{4}G survey which has 256 galaxies morphologically classified as early-type. We use HyperLeda (Makarov et al. 2014) database to collect basic information on these galaxies. Next we cross match this sample with SDSS data from Knapen et al. (2014), where authors have done cross-matching with SDSS DR7 and DR8 data release with S^{4}G survey. This SDSS-S^{4}G cross-match gives 1657 galaxies of various morphological types out of which 150 have early-type galaxies. We use various techniques (see Chapter 3) to detect dust features in these galaxies and our final sample consist of 58 galaxies with variety of dust features. Of these 58 galaxies, 1 is E-S0 galaxy, 1 is E galaxy, 15 are S0 galaxies and 41 are S0-a. The full sample of 58 galaxies is listed in Table 4.1.

Table 2.2: The RC3 parameters for S0 galaxies.

Galaxy	T	$\log(D_{25})$	r	$3.6_{\mu m}$
IC 0719	-1.9	1.08	12.79	12.28
IC 0796	-0.2	1.16	12.97	13.01
IC 1024	-2	1.04	17.79	12.44
IC 3102	-0.9	1.30	12.21	11.73
NGC 0063	-3.4	1.23	10.75	11.84
NGC 1032	-0.4	1.55	11.72	10.99
NGC 2681	-0.4	1.59	11.00	10.17
NGC 2685	-1	1.63	11.54	10.96
NGC 2764	-1.8	1.06	12.80	12.19
NGC 3032	-1.9	1.15	12.52	12.23
NGC 3166	-0.3	1.65	10.49	9.85
NGC 3413	-1.5	1.30	12.89	13.08
NGC 3489	-1.2	1.53	10.95	10.04
NGC 3593	-0.4	1.67	11.53	9.99
NGC 3619	-0.9	1.59	11.84	11.56
NGC 3626	-0.9	1.46	11.29	10.76
NGC 3682	-0.1	1.34	12.19	11.71
NGC 3773	-2	1.08	16.04	13.17
NGC 3900	-0.2	1.40	11.85	11.33
NGC 3928	-4.8	1.13	12.39	12.13
NGC 4117	-2.1	1.20	12.85	12.71
NGC 4118	-1	0.84	15.21	12.73
NGC 4138	-0.8	1.46	14.95	10.79
NGC 4220	-0.3	1.51	11.58	10.78
NGC 4245	-0.1	1.40	11.41	10.90
NGC 4293	-0.3	1.79	11.64	10.06

Continued on next page

Table 2.2– *Continued from previous page*

Galaxy	T	$\log(D_{25})$	r	$3.6_{\mu m}$
NGC 4309	-0.9	1.28	12.94	12.51
NGC 4310	-0.9	1.28	12.61	12.25
NGC 4324	-0.9	1.47	11.70	11.17
NGC 4336	-0.1	1.18	12.64	12.52
NGC 4344	-2.1	1.12	12.73	12.70
NGC 4405	-0.1	1.22	12.19	11.93
NGC 4457	0.4	1.44	10.90	10.21
NGC 4460	-0.9	1.59	12.16	11.61
NGC 4531	-0.5	1.48	12.00	11.42
NGC 4599	0.4	1.23	12.58	12.34
NGC 4641	-2	1.10	13.25	13.22
NGC 4680	0	1.13	12.63	12.79
NGC 4691	-0.3	1.48	11.54	10.81
NGC 4694	-2	1.30	12.10	11.55
NGC 4710	-0.9	1.62	17.28	10.25
NGC 4753	-1.2	1.81	10.73	9.26
NGC 4866	-0.1	1.76	11.69	10.63
NGC 5311	-0.1	1.30	12.31	11.76
NGC 5353	-2	1.37	11.05	10.92
NGC 5354	-2.1	1.48	11.67	10.81
NGC 5360	0.1	1.04	14.59	13.57
NGC 5363	-0.4	1.62	15.15	9.54
NGC 5422	-1.4	1.44	12.06	11.48
NGC 5587	-0.1	1.39	12.76	12.54
NGC 5631	-1.9	1.28	11.56	10.95
NGC 5689	-0.4	1.56	11.73	11.09
NGC 5750	-0.4	1.42	11.99	11.19
NGC 5953	0	1.16	12.27	11.54
NGC 6014	-1.8	1.24	12.79	12.35
NGC 7465	-1.8	1.02	11.26	12.00
UGC 05695	-1	1.11	14.13	14.21
UGC 10803	-1	1.11	12.73	12.49

Notes. The first three parameters are from the HyperLeda database and the last two are from the S^{4}G and SDSS surveys. Column (1) give the name of galaxies that are rich in dust from the S^{4}G and SDSS sample. Column (2) indicates the morphological type code of each galaxy. Column (3) is the apparent major axis diameter 25 mag.arcsec^{-2}; D_{25} is in units of $0.1'$. Columns (4) and (5) is the apparent magnitude r and $3.6_{\mu m}$ mag, respectively.

We used the r and i bands images along with 3.6 and 4.5 μm IRAC channels, respectively for our work. With this cross-match, we intend to identify unusual features across a broad wavelength range. All of the techniques used for this features are well discuses in details in Chapter 3.

Chapter 3

Data Analysis

In this chapter, we describe data analysis techniques to investigate the presence of molecular gas in S0 galaxies. We discuss one of the most powerful technique known as *colour maps*, which is used to detect many features including molecular gas by measuring dust extinction.

3.1 Detection techniques

Optical observations such as images from SDSS, thanks to their high spatial resolution, are essential for establishing the presence and distribution of dust and gas in galaxies as most of dust re-emits in IR. We employed a variety of techniques to detect dust and other features. We started using features of a tool *SAOImage ds9* which astronomers often use for astronomical imaging and data visualization (Joye & Mandel 2003), to display the images of each galaxy to examine various features.

The unsharp-masking, galaxy model division, and colour map are other useful techniques to detect dust and other features using optical and infrared images. These techniques have been used by many authors including, Rahman et al. (2011), Ebneter et al. (1988), Sheth et al. (2000), Goudfrooij et al. (1994), Patil et al. (2007) and Kulkarni et al. (2014). Dust and other faint structures are hidden onto the bright background of the galaxy which makes them particularly difficult to detect. In order to search these structures and isolate them within the galaxy, it is necessary to first subtract smooth model of the underlying galaxy. *Unsharp Masking* is a technique where smooth image of galaxy made using Image Reduction and Analysis Facility (IRAF; Tody 1986) `boxcar` task and subtracted from the observed image reveals several structures including dust lane/patch and other features. Another way to identify dust structure in galaxy images is *structure map* technique proposed by Pogge & Martini (2002). *Structure maps* enhance structure as fine as the scale of the point spread function in an image and are well suited to the identification of narrow dust lanes and emission-line gas in nearby galaxies.

A commonly used technique to detect dust is by inspecting colour index images or known as *colour maps* in which dust shows up as distinct, reddened structures. This technique reveals various hidden features such as dust lane, ring, patches and other features within a galaxy. We used this technique for the work presented in this thesis by combing optical (from SDSS) and near-IR (S^4G) images to obtain various colour maps. We have constructed $(r-3.6)$, $(i-4.5)$, and $(3.6-4.5)$ colour maps to examine dust structures and its morphologies.

3.2 Colour Maps

The most direct way of looking for dust using broad-band imaging is to construct a colour map from images of a galaxy obtained in two different filters. We have adopted the following procedure to obtain optical-IR colour maps (i.e., $(r-3.6)$ and $(i-4.5)$ maps):

- The images provided by S^4G survey in 3.6 and 4.5 micron are in flux units (i.e., MJy.sr^{-1}) while SDSS images in r and i filters are in counts per second (ADU/s). We have used conversion factor obtained from header keyword `FLUXCONV`, to convert from flux unit to counts per second.
- Once images are in same unit, we made a careful estimation of sky background and subtracted from each image.
- IRAF tasks `GEOMAP` and `GEOTRAN` were used to accurately align images in various filters using 3.6 micron as reference image. These tasks not only geometrically aligned images but also rescale counts by matching pixel scale of individual images.
- Next step is to degrade the image which has the PSF with the smaller FWHM to the PSF with the larger FWHM. In our case, PSF of optical (r and i) images were degraded to match with IR (3.6 and 4.5 micron) images.
- Final step is to divide the r (or i) image by the 3.6 (or 4.5) micron image and convert the quotient image to the magnitude scale which we call $(r-3.6)$ or $(i-4.5)$ colour map.

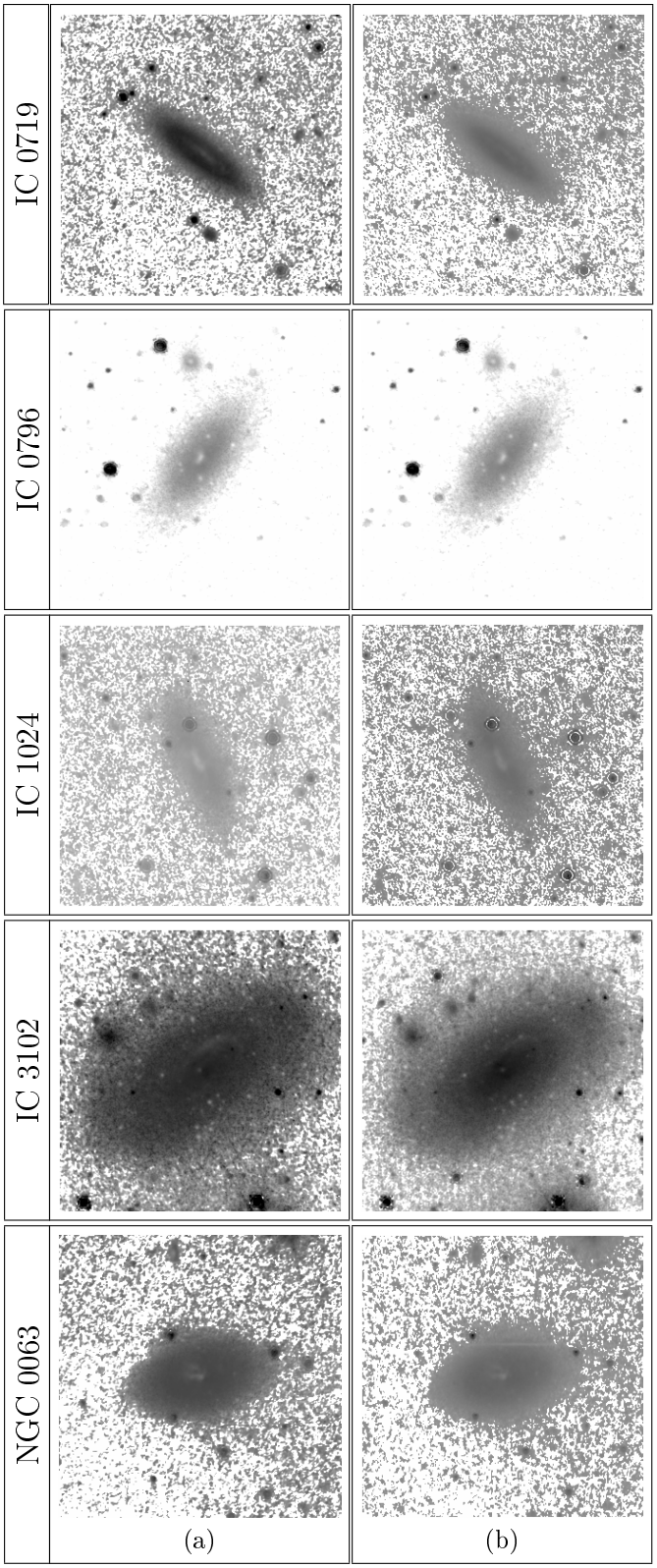

Figure 3.1: The panel (a) show colour maps of $(r-3.6)$ and panel (b) show $(i-4.5)$ colour maps, with image size of 225.75×225.75 arcsec. The gray regions indicate the redder dust origins. In these images the North is up and East is to the left.

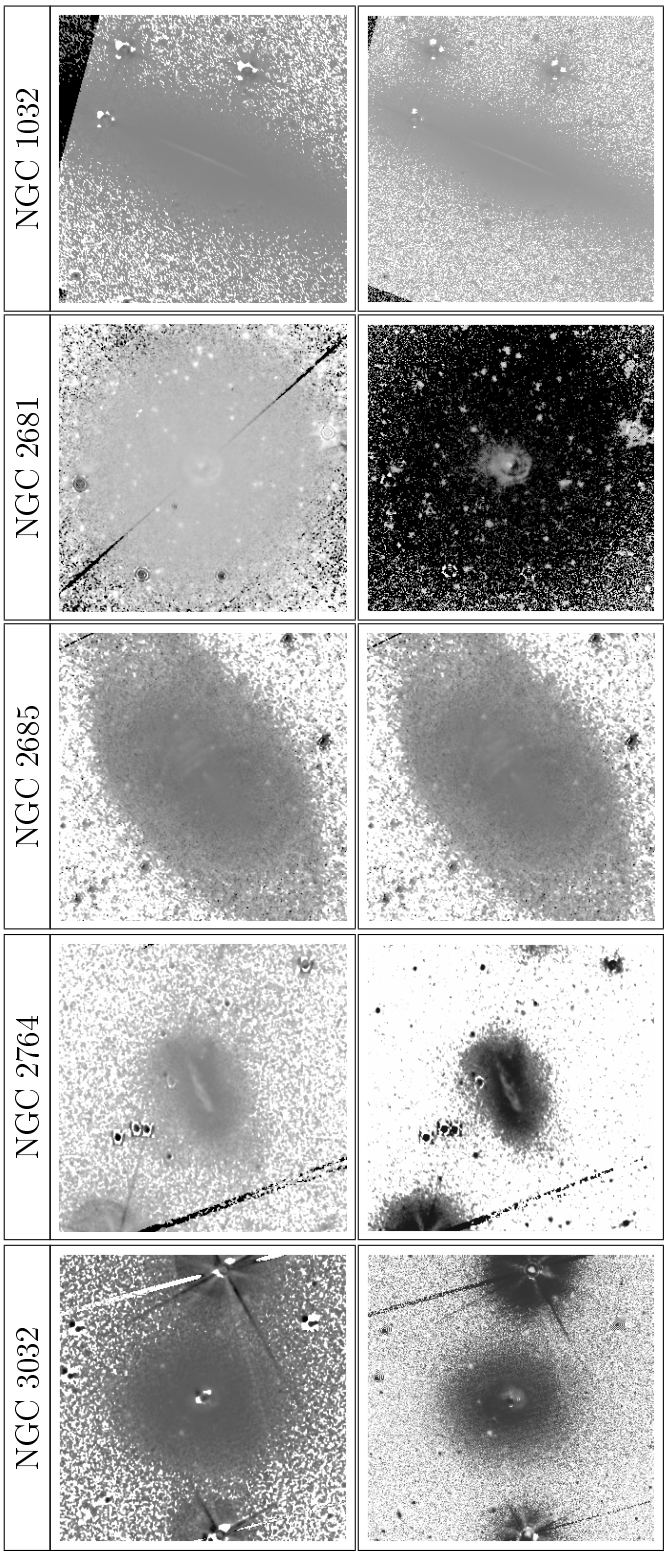

Figure 3.1: *Continued*

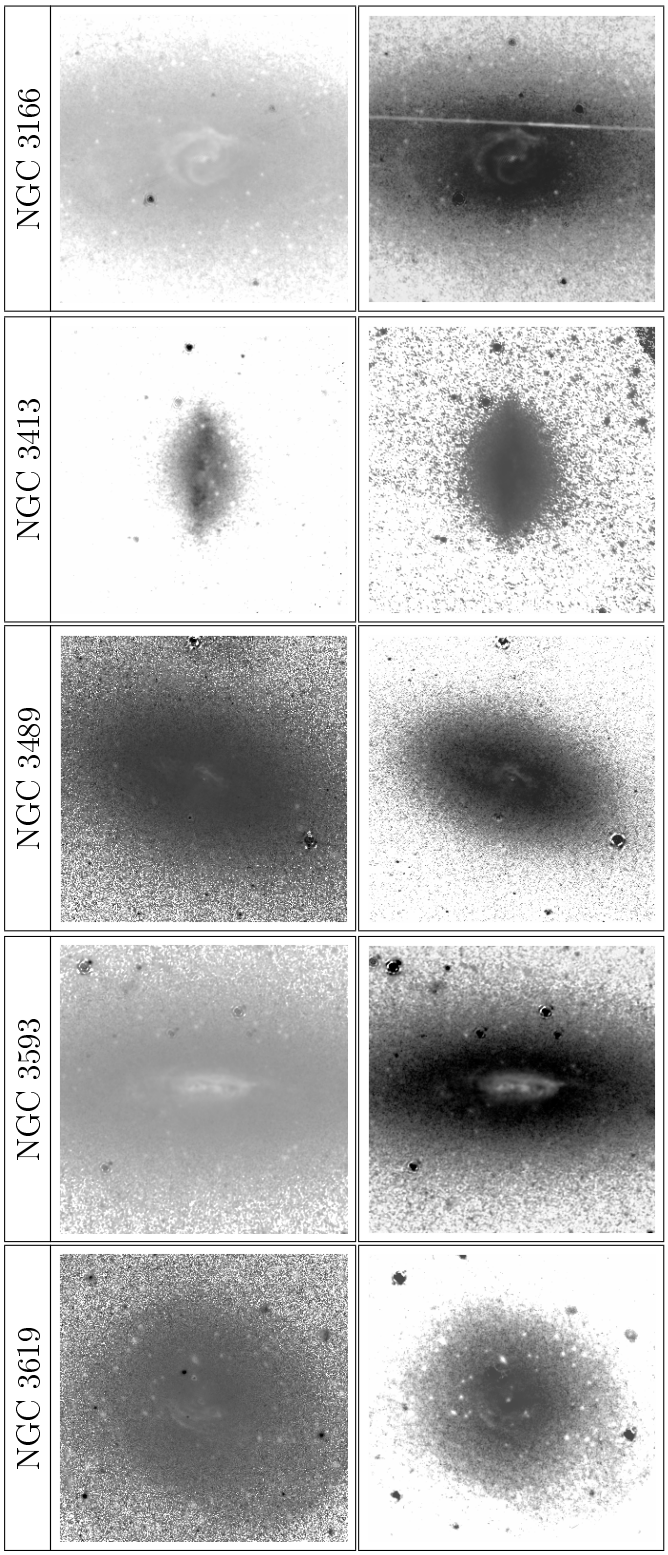

Figure 3.1: *Continued*

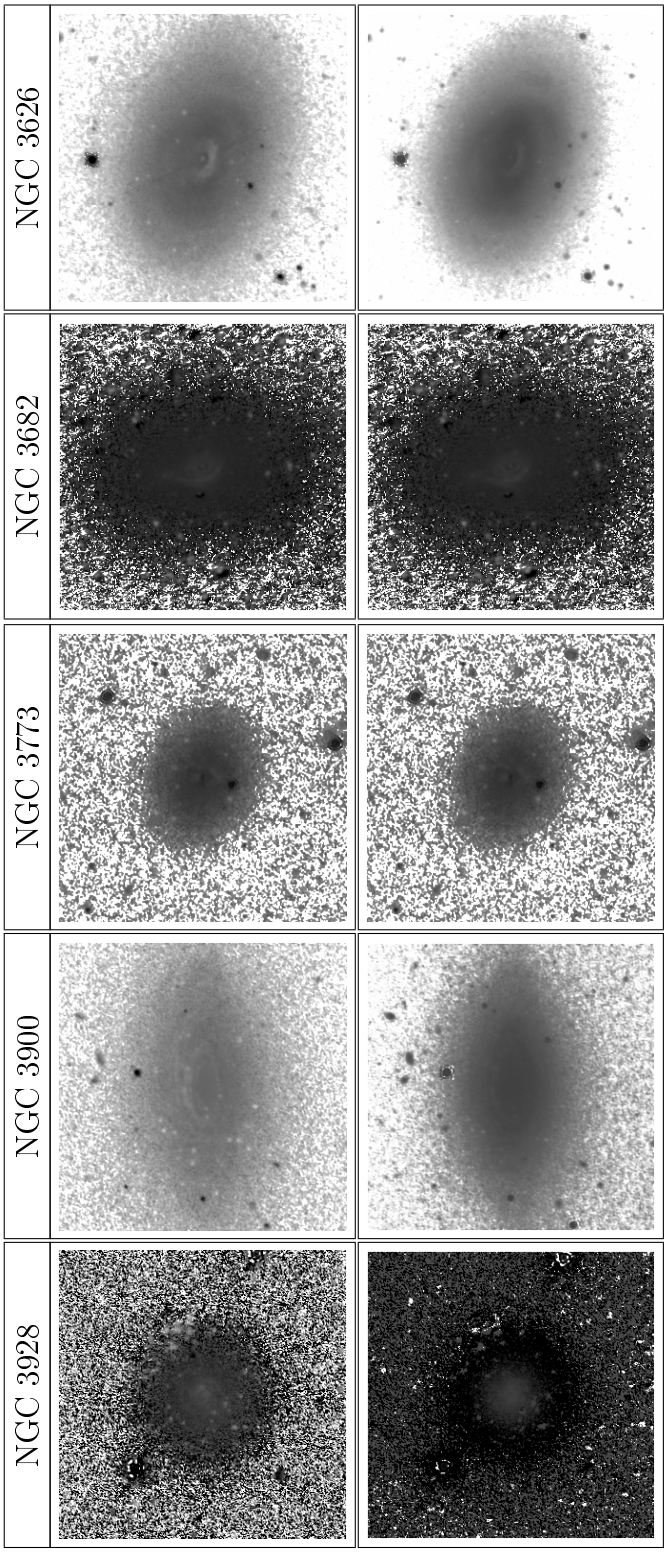

Figure 3.1: *Continued*

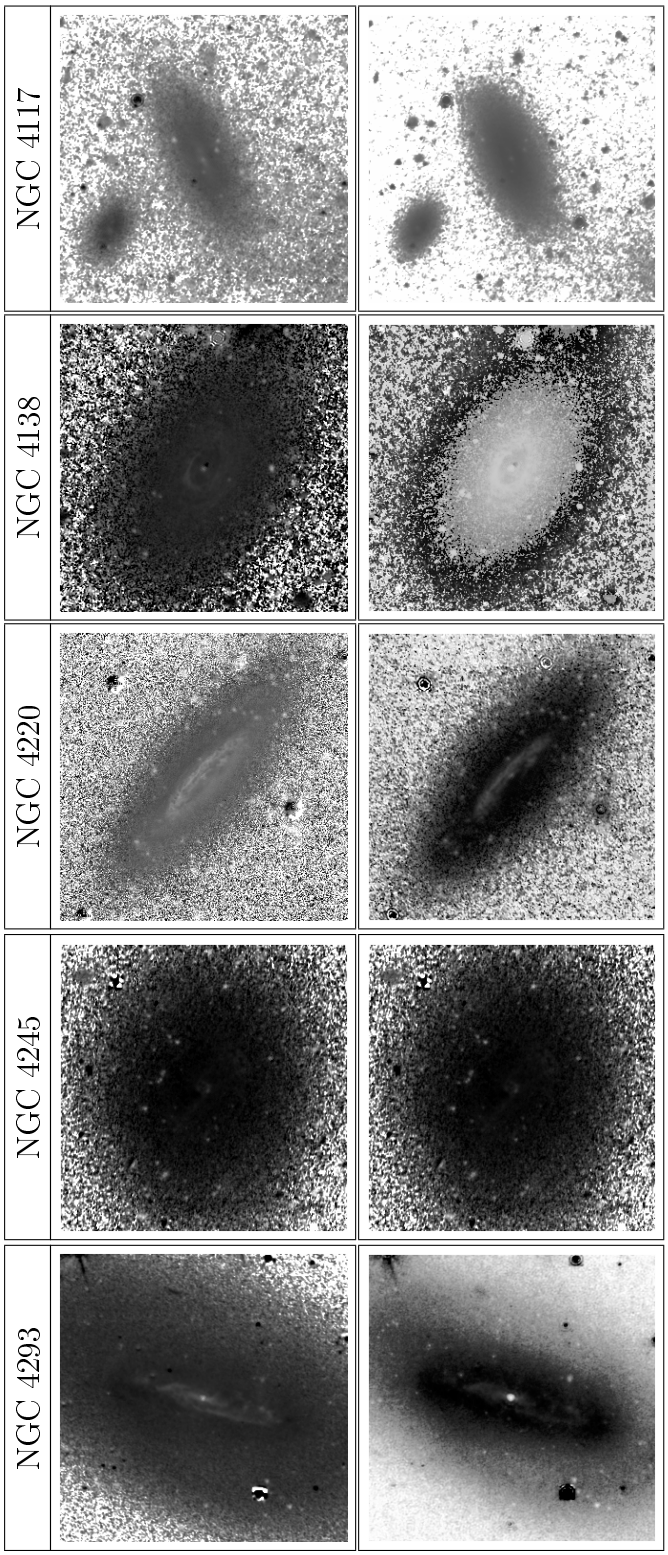

Figure 3.1: *Continued*

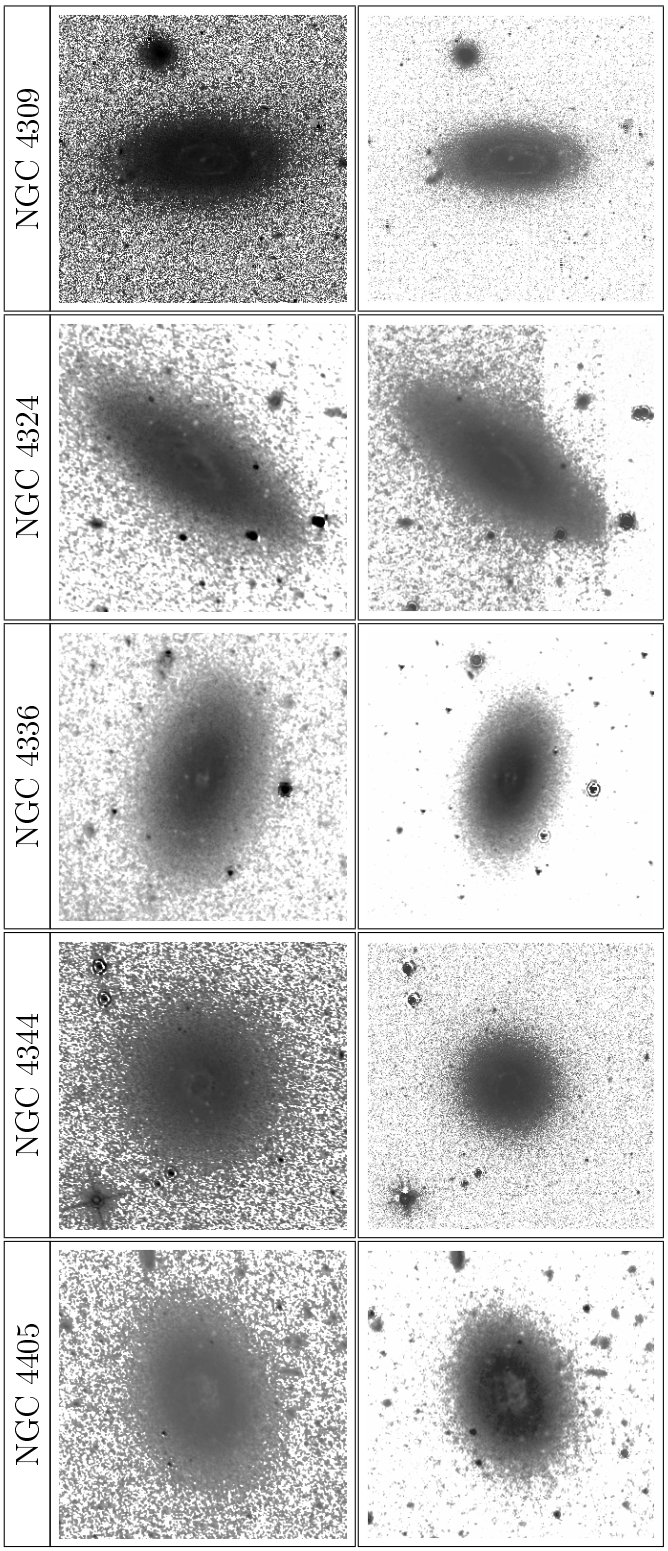

Figure 3.1: *Continued*

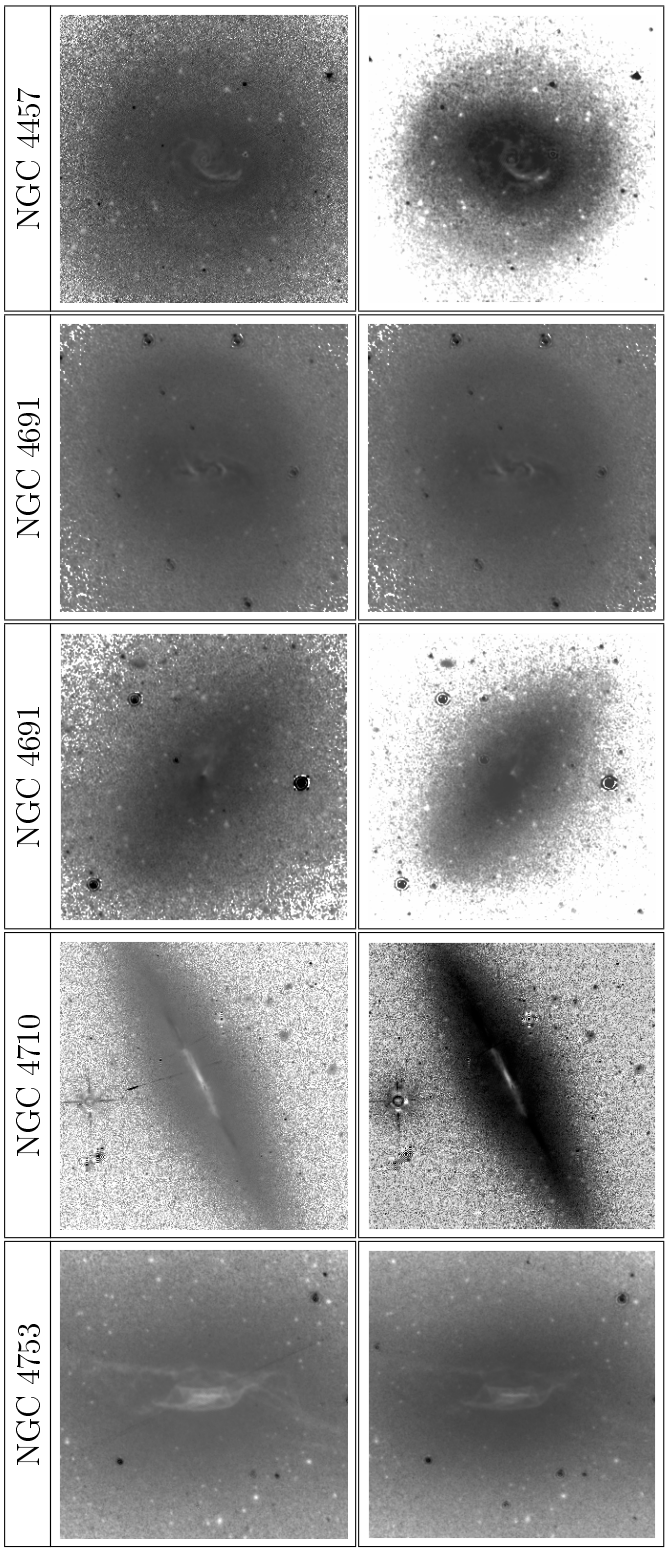

Figure 3.1: *Continued*

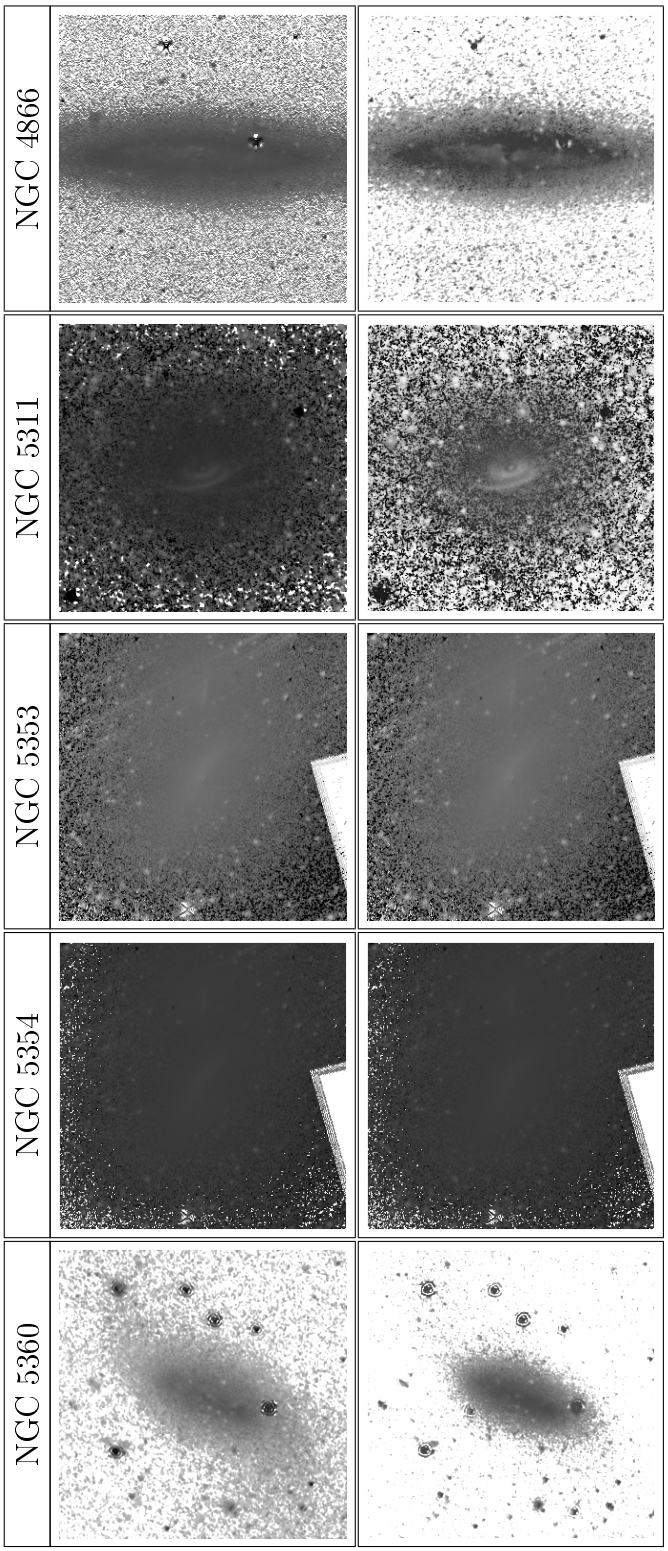

Figure 3.1: *Continued*

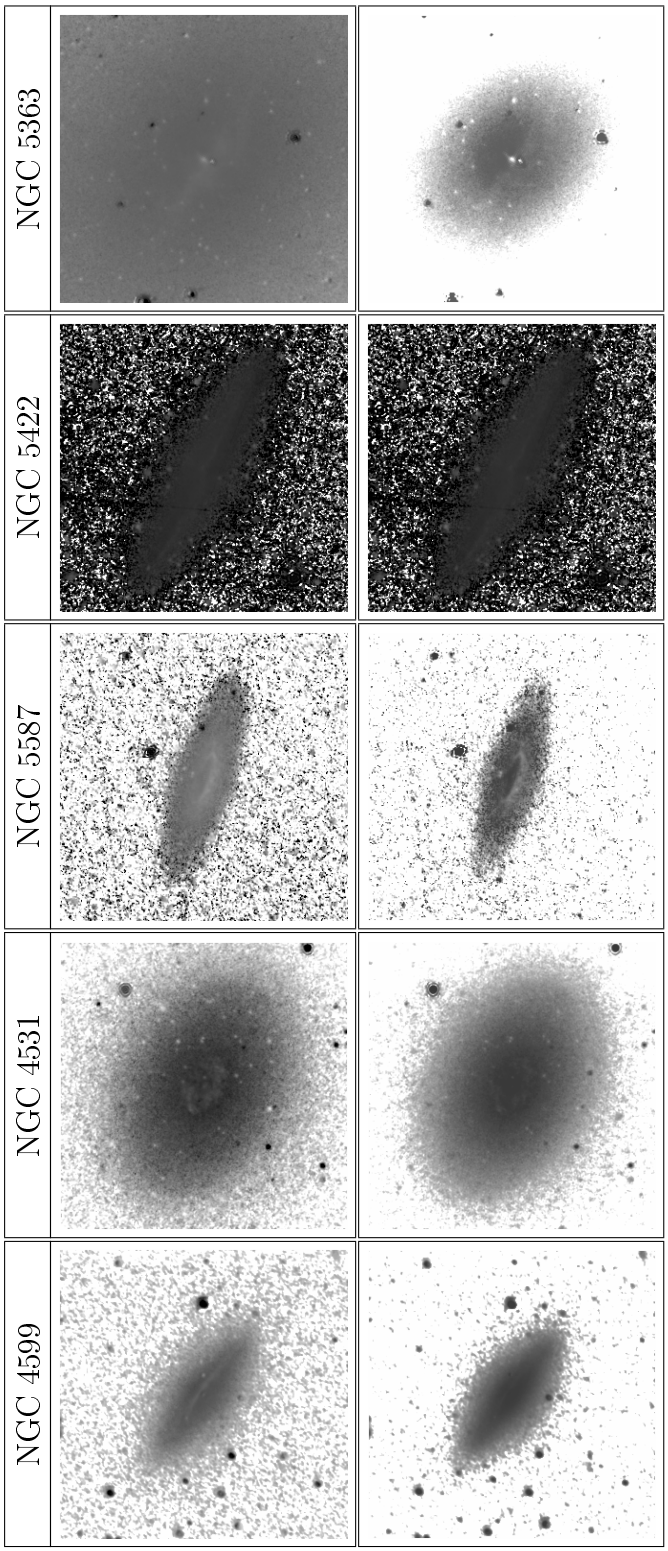

Figure 3.1: *Continued*

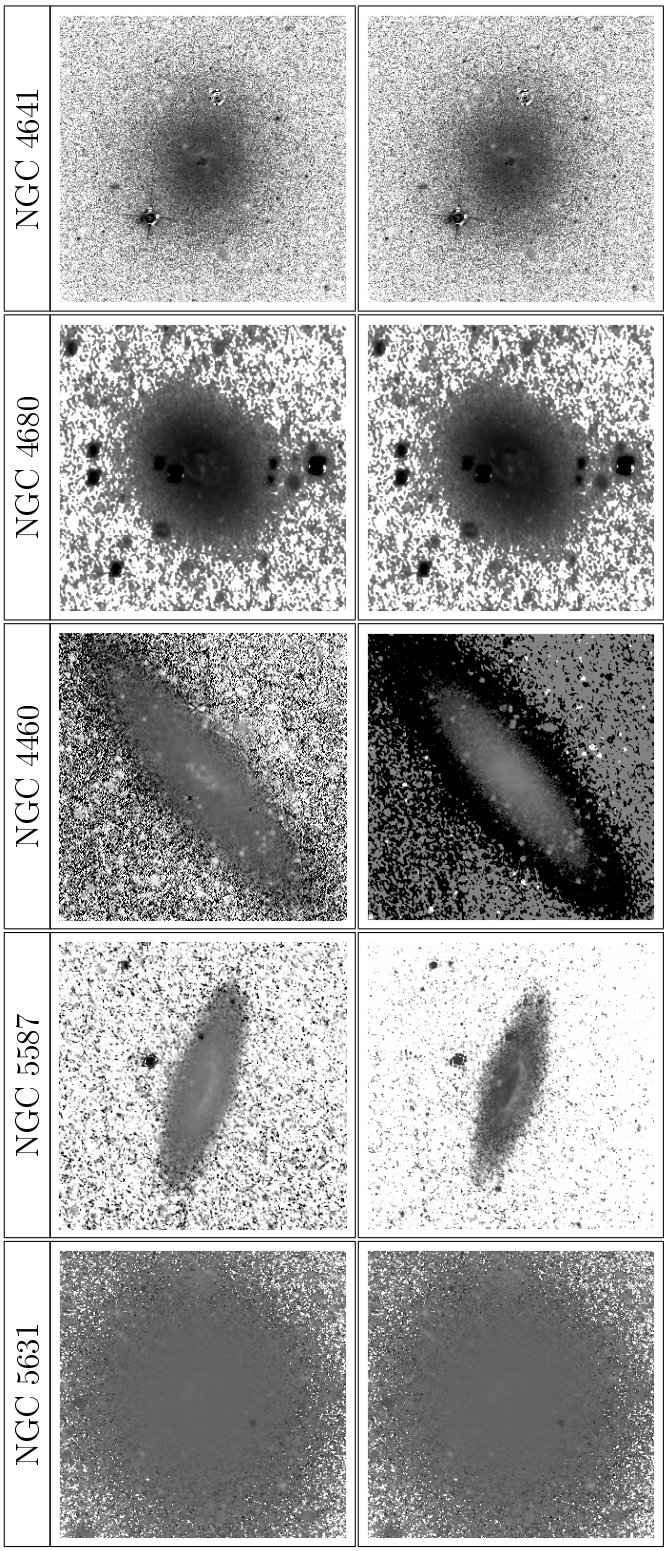

Figure 3.1: *Continued*

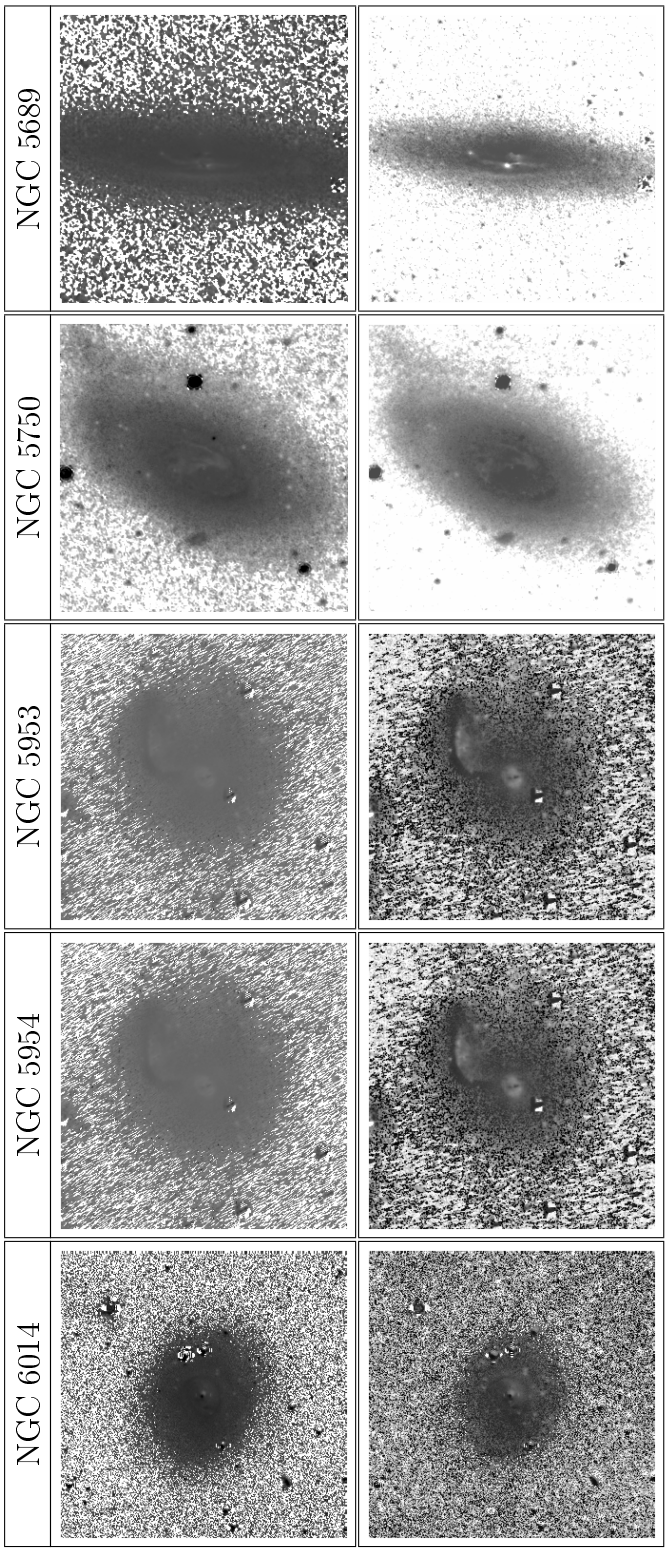

Figure 3.1: *Continued*

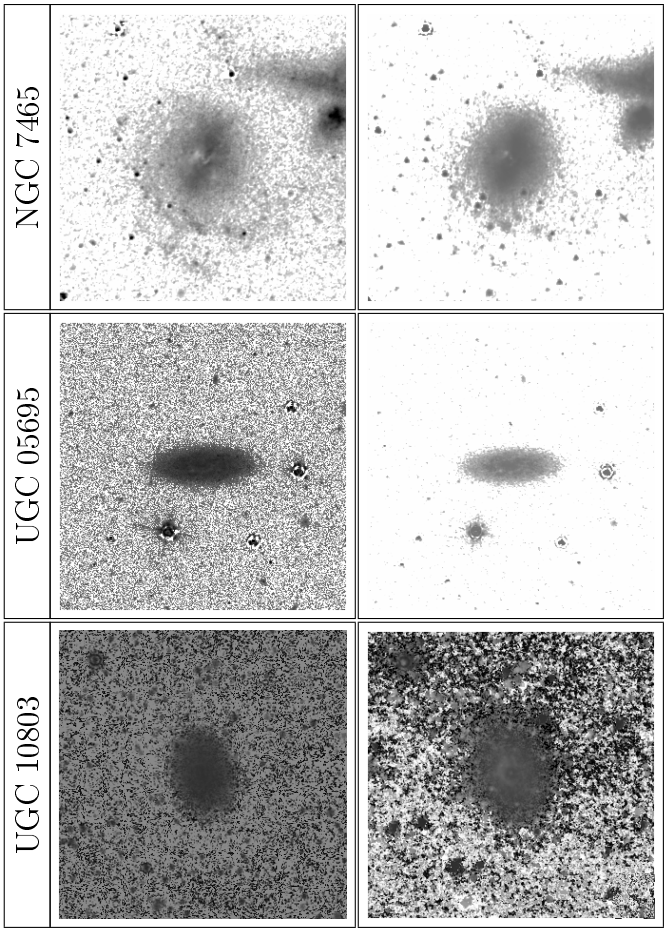

Figure 3.1: *Continued*

The $(r-3.6)$ and $(i-4.5)$ colour maps are presented in Figure 3.1(a) and Figure 3.1(b). The main effect of constructing these colour maps was to remove the smooth background provided by the longer wavelength from the shorter wavelength images, and to highlight the molecular gas affected regions. As a result this technique enhanced the appearance of molecular gas feature anywhere in the galaxy.

We follow the same procedure to obtain $(3.6-4.5)$ colour maps. It is very difficult to detect dust absorption in 3.6 and 4.5 micron bands as it re-emits at these wavelengths. However, for five galaxies we detect dust in $(3.6-4.5)$ colour map (see Figure 3.2) and these galaxies are NGC 1032, NGC 2681, NGC 3900, NGC 4710 and NGC 5953.

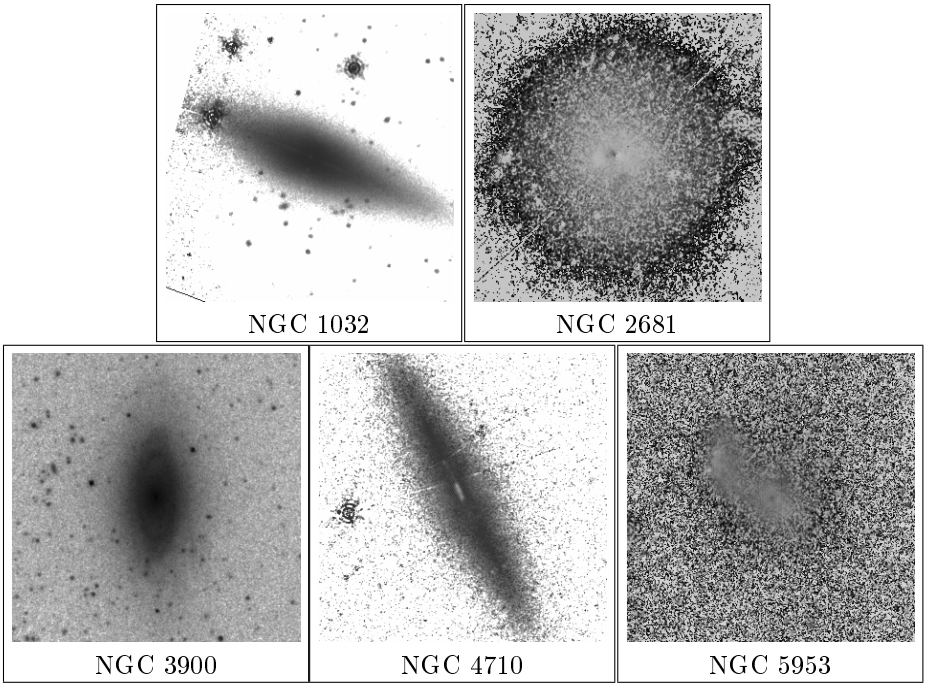

Figure 3.2: The $(3.6-4.5)$ colour maps of the S0 galaxies with a dust detected in near-IR wavelengths. The size of each panel is 225.75×225.75 arcsec. The North is up, East is to the left.

3.3 Dust morphology

We determine dust morphology by inspecting $(r-3.6)$ and $(i-4.5)$ colour maps using ds9. We have considered all the dust structures described in literature. From these structures, we have recognized five morphological features: the disorganized dust patches (d), dust ring (r), spiral dust (s), dust lane (l), and transition case between ring and non-ring gas (t; see Figure 3.3).

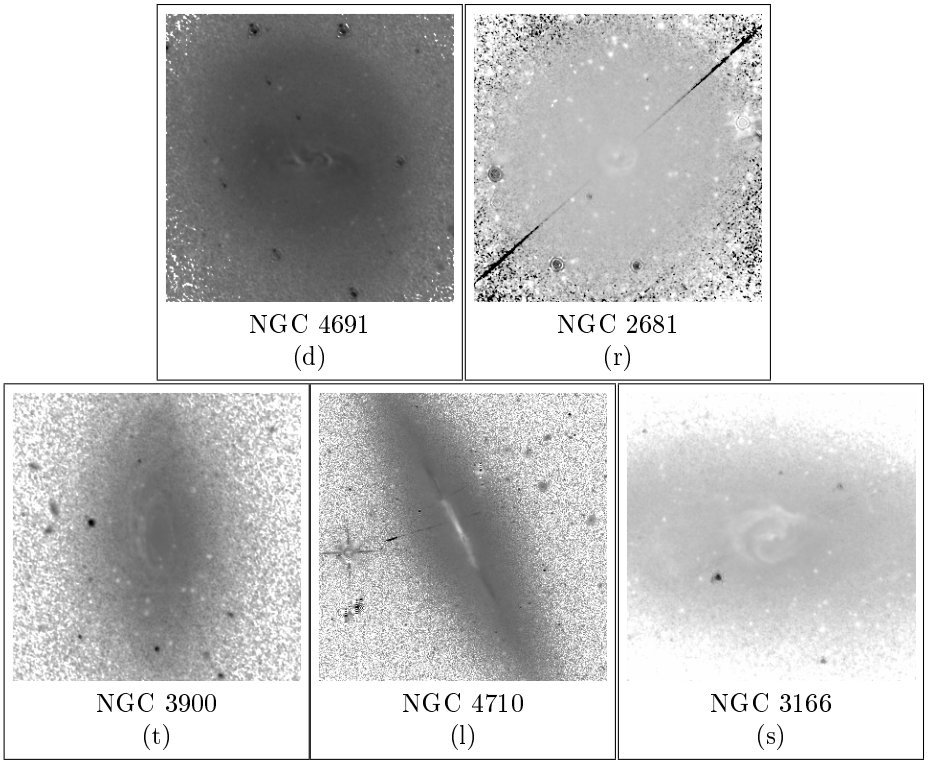

Figure 3.3: Various dust morphology as seen in our S0 sample from colour maps. See in section 3.3 for details.

The disorganized dust patches doesn't show clear structure in a host galaxy. Dust ring are the small circular bands of dust with one or more circular pattern around the center of the galaxy. The spiral dust is the dust winding in a continuous and gradually widening either around a central point on a flat plane of galaxy. A dust lane is one with narrow line run across galaxy along the major axis. The final structure is a t-morphology, these structures are the dust transition between rings and non-rings. We find 50% of the sample had disturbed dust patches (d), (∼11%) dust ring (r), three (∼5%) spiral dust (s), (∼17%) was the dust lane (l), and (∼17%) transition case between ring and non-ring dust (t) morphology from both maps. These dust morphologies are summarized in Column 2 of Table 3.1.

Table 3.1: The Dust morphologies of S0 galaxies.

Object Name	Dust Morph.
IC 0719	l
IC 0796	d
IC 1024	d
IC 3102	l
NGC 0063	d

Continued on next page

Table 3.1– *Continued from previous page*

Object Name	Dust Morph.
NGC 1032	l
NGC 2681	r
NGC 2685	l
NGC 2764	l
NGC 3032	r
NGC 3166	s
NGC 3413	d
NGC 3489	d
NGC 3593	d
NGC 3619	d
NGC 3626	r
NGC 3682	t
NGC 3773	d
NGC 3900	t
NGC 3928	d
NGC 4117	d
NGC 4118	t
NGC 4138	t
NGC 4220	t
NGC 4245	d
NGC 4293	d
NGC 4309	t
NGC 4310	d
NGC 4324	r
NGC 4336	d
NGC 4344	t
NGC 4405	d
NGC 4457	s
NGC 4460	d
NGC 4531	d
NGC 4599	l
NGC 4641	d
NGC 4680	s
NGC 4691	d
NGC 4694	d
NGC 4710	l
NGC 4753	d

Continued on next page

Table 3.1– *Continued from previous page*

Object Name	Dust Morph.
NGC 4866	d
NGC 5311	t
NGC 5353	l
NGC 5354	d
NGC 5360	d
NGC 5363	d
NGC 5422	l
NGC 5587	t
NGC 5631	l
NGC 5689	t
NGC 5750	d
NGC 5953	d
NGC 6014	r
NGC 7465	d
UGC 05695	d
UGC 10803	r

Notes. Column (1) give the name of galaxies and Column (2) indicates the molecular gas mophologies from the indivisual galaxies.

Dust morphologies are useful to study origin of dust in galaxies as well as provides clues to host galaxy formation. There are various scenario describe in literature. Kaviraj et al. (2012) suggest that the merger origin of these galaxies which largely involves minor mergers between dry early-type galaxy and gas-rich dwarf. Most of these galaxies reside in lower density environments and show close correspondence between dust and cold gas (Knapp 1999). This makes instructive to explore the properties of the gas of early-type galaxies.

Chapter 4

Optical-IR colour excess as a tracer of molecular gas

In this chapter, we investigate possible correlation between optical-IR colour excess and mass of molecular gas measured using CO emission available in the literature. The optical-IR colour excess show a trend with some scatter.

4.1 Colour excess measurement

There are many methods exists in literature to estimate colour excess in the dusty region. For example, colour excess in $(r-3.6)$ can be measured by

$$E(r-3.6) = (r-3.6)_{\rm observed} - (r-3.6)_{\rm intrinsic}. \tag{4.1}$$

Where $E(r-3.6)$ is the difference between the observational apparent colour $(r-3.6)_{\rm observed}$ and the intrinsic colour $(r-3.6)_{\rm intrinsic}$. There are various ways to get $(r-3.6)_{\rm intrinsic}$, i.e., by modeling the dust free region. However, for this work we adopted simple strategy.

We measured the colour excess in the dusty region by comparing the colour of its surrounding areas, i.e., regions of the galaxy not affected by dust. For this purpose, we use a polygon aperture to enclose the entire dusty region on the r, 3.6, i and 4.5 images separately to extract magnitudes and various square apertures in a neighbouring region free of gas. The mean colour excess is obtain in $(r-3.6)$ and $(i-4.5)$ and are listed in Table 4.1.

Table 4.1: Colour-excess and molecular gas masses for S0 galaxies

Object Name	$E(r-3.6)$ (mag)	$E(i-4.5)$ (mag)	log M_{H_2} $(M_\odot)$	Source
IC 0719	0.19	0.17	8.26 (0.04)	1
IC 0796	0.17	0.13	-	-
IC 1024	0.56	0.41	8.16 (0.02)	1
IC 3102	0.13	0.09	$<$7.23	1
NGC 0063	0.50	0.37	-	-
NGC 1032	0.12	0.09	-	-
NGC 2681	0.34	0.26	8.07	3
NGC 2685	0.03	0.01	7.29 (0.080)	1
NGC 2764	0.72	0.59	9.19 (0.02)	1
NGC 3032	0.55	0.47	8.41 (0.01)	2
NGC 3166	0.44	0.34	8.22	6
NGC 3413	0.54	0.34	$<$7.90	5
NGC 3489	0.13	0.08	7.2 (0.06)	1
NGC 3593	0.70	0.62	8.34	5
NGC 3619	0.59	0.43	8.28 (0.05)	1
NGC 3626	0.04	0.01	8.26	1
NGC 3682	0.92	0.79	8.27	6
NGC 3773	0.07	0.02	-	-
NGC 3900	0.79	0.59	-	-
NGC 3928	0.21	0.19	-	-
NGC 4117	0.04	0.01	7.7	2
NGC 4118	0.10	0.02	-	-
NGC 4138	0.25	0.16	8.34	5
NGC 4220	0.32	0.26	-	-
NGC 4245	0.21	0.12	-	-
NGC 4293	0.14	0.09	8.06	6
NGC 4309	0.09	0.02	8.05 (0.02)	1
NGC 4310	0.21	0.18	-	-
NGC 4324	0.39	0.24	7.96 (0.05)	1
NGC 4336	0.62	0.49	-	-
NGC 4344	0.18	0.10	7.38	4
NGC 4405	0.51	0.36	-	-
NGC 4457	0.08	0.01	9.32	5
NGC 4460	0.17	0.10	-	-
NGC 4531	0.05	0.01	7.26	4
NGC 4599	0.39	0.29	-	-
NGC 4641	0.21	0.18	-	-

Continued on next page

Table 4.1– *Continued from previous page*

Object Name	$E(r-3.6)$ (mag)	$E(i-4.5)$ (mag)	log M_{H_2} $(M_\odot)$	Source
NGC 4680	0.41	0.41	-	-
NGC 4691	0.11	0.09	8.95	6
NGC 4694	0.01	0.01	8.01 (0.03)	1
NGC 4710	0.36	0.29	8.72 (0.01)	1
NGC 4753	0.93	0.81	8.55 (0.03)	1
NGC 4866	0.19	0.13	-	-
NGC 5311	0.09	0.02	-	-
NGC 5353	0.50	0.36	$<$8.12	1
NGC 5354	0.20	0.11	-	-
NGC 5360	0.22	0.12	-	-
NGC 5363	0.31	0.21	$<$8.73	5
NGC 5422	0.10	0.06	$<$7.78	1
NGC 5587	0.08	0.01	-	-
NGC 5631	0.20	0.09	$<$7.68	1
NGC 5689	0.07	0.03	-	-
NGC 5750	0.41	0.32	-	-
NGC 5953	0.53	0.37	8.75	6
NGC 6014	0.40	0.25	8.77 (0.02)	1
NGC 7465	0.12	0.09	8.79 (0.02)	1
UGC 05695	0.23	0.18	-	-
UGC 10803	0.49	0.30	-	-

Notes. Column (1) give an object name, columns (2) and (3) gives colour excess in $(r-3.6)$ and $(i-4.5)$, respectively. Column (4) gives the molecular gas masses taken from the literature. The final column (5) indicates the source which we taken masses from. Mass data: (1) Young et al. (2011), (2) Wei et al. (2010), (3) Braine & Combes (1992), (4) Boselli et al. (1995), (5) Thronson Jr et al. (1989), and (6) Wiklind & Henkel (1989).

4.2 Measurement of molecular gas mass

The molecular gas mass measurements used here are taken from Young et al. (2011) and reference therein. Young et al. (2011) carried out a survey of CO J = 1-0 and J = 2-1 emission detected in the 260 early-type galaxies of the volume-limited ATLAS^{3D} sample. This survey is the largest volume-limited CO survey with an objective to connect the star formation and assembly histories of cold gas content of early-type galaxies. These galaxies were observed by the Spanish telescope IRAM 30 meter at Pico Veleta. This telescope observe ^{12}CO(1-0) and (2-1) emission simultaneously using the *SIS* receivers in the wobbler switching mode, with reference positions offset by $\pm 100''$ in azimuth. The beam FWHM is $21.6''$ and $10.8''$

at the two frequencies, respectively. The 1 MHz filter bank backend gave an effective total bandwidth of 512 MHz and a raw spectral resolution of 2.6 km.s^{-1} for CO(1–0). The 4 MHz filter bank gave an effective total bandwidth of 1024 MHz and a raw spectral resolution of 5.2 km.s^{-1} for CO(2-1), and both bandwidth had a velocity of 1330 km.s^{-1}. See Young et al. (2011) for details on observations, data reduction and mass determination.

The intensities, I_J, were integrated by summing the spectrum over the velocity for each galaxy. For the weak or absent line emissions, the velocity range was 300 km.s^{-1} centered on the systemic velocity of stellar absorption lines as measured from the old data from SAURON. Then for the obvious detections, the integrated velocity range covered the real emission.

Integrated intensity was used to estimate the total mass of the molecular gas using its relationship with column density given by $N(H_2) = 3.0 \times 10^{20} I_{1-0}$. This relation converts an integrated intensity to a gas column density averaged over the beam and the multiplication by the beam area gives the total gas mass as

$$\frac{M_{H_2}}{M_\odot} = 6.0 \times 10^4 \left(\frac{D}{\mathrm{Mpc}}\right)^2 \left(\frac{\int T_{mb} dv}{\mathrm{K\,km.s^{-1}}}\right), \tag{4.2}$$

where the intensity are quoted as main beam brightness temperature T_{mb}. This temperature is converted by dividing the antenna temperatures T_A^* by the ratio of beam and forward efficient, $B_{\mathrm{eff}}/F_{\mathrm{eff}} = 0.78$ at 2.6 mm and 0.63 at 1.3 mm. The conversion from the main beam temperature to flux density in Jy is 4.73 Jy.K^{-1} for the 30 m beam at both frequencies.

4.3 Optical-IR colour excess and molecular gas mass

As it was stated before optical-IR colour map and colour excess can be used as the tracers of molecular gas presence in early-type galaxies, it would be interesting to investigate possible correlations between the molecular gas mass content and optical-IR colour excess. We find that 38 out of 58 S0 galaxies for which we obtained colour maps and hence were able to measure colour excess have CO detection and have mass measurements from Young et al. (2011) and references therein.

The CO masses and their limits for our sample of S0 galaxies are listed in the 4th column of Table 4.1. Before we investigate any correlation between the M_{H_2} and optical-IR colour excess, we should indicate that for non-detected galaxies, the quoted mass limits correspond to three times the statistical uncertainty in an integral over the assumed line-width and quoted error is a 1σ formal uncertainty assuming a binomial distribution.

If optical-IR colour map and optical-IR colour excess are tracers of molecular gas, one

would be expected to see some trend between optical-IR colour excess and molecular gas mass. With this intention, we plotted $(r-3.6)$ colour excess on the x-axis and M_{H_2} measured from CO on the y-axis in Figure 4.1 for our sample of S0 galaxies. For colour excess $(r-3.6) > 0.18$, we see a trend between $(r-3.6)$ colour excess and M_{H_2} with some scatter that has a slope of 0.84 $M_\odot$/mag.

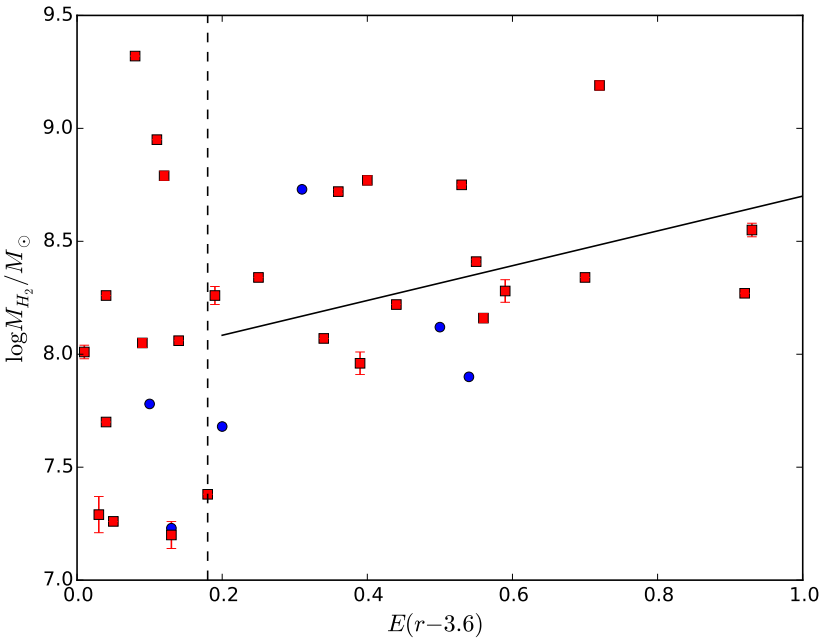

Figure 4.1: CO mass versus $(r-3.6)$ colour excess of dust in S0 galaxies. Lower limit detections are shown with blue solid circles.

We do not see any trend for small colour excess $(r-3.6) < 0.18$. This result might be due to an inaccurate measurement of colour excess, where we had to perform a measurement process more than expected in order to record a final mean value. However, we've planned to deploy more accurate techniques on our future study in order to improve the measurements of colour excess of this topic (see the next chapter). We see similar trend when $(i-4.5)$ colour excess plotted against M_{H_2} measured from CO in Figure 4.1 (see Figure 4.2)

Sheth et al. (2000) has presented various optical-IR colour maps and found the dust extinction peaks match the peaks seen in CO-emission. These authors also find qualitative agreement between the CO emission and dust extinction distributions, indicating that CO is a reliable tracer of the dense gas distribution (Sheth et al. 1998). In this work for the colour excess $(r-3.6) > 0.18$, we have shown, for the first time that the mass of molecular gas obtained by CO is correlated to colour excess measured from $(r-3.6)$ colour maps.

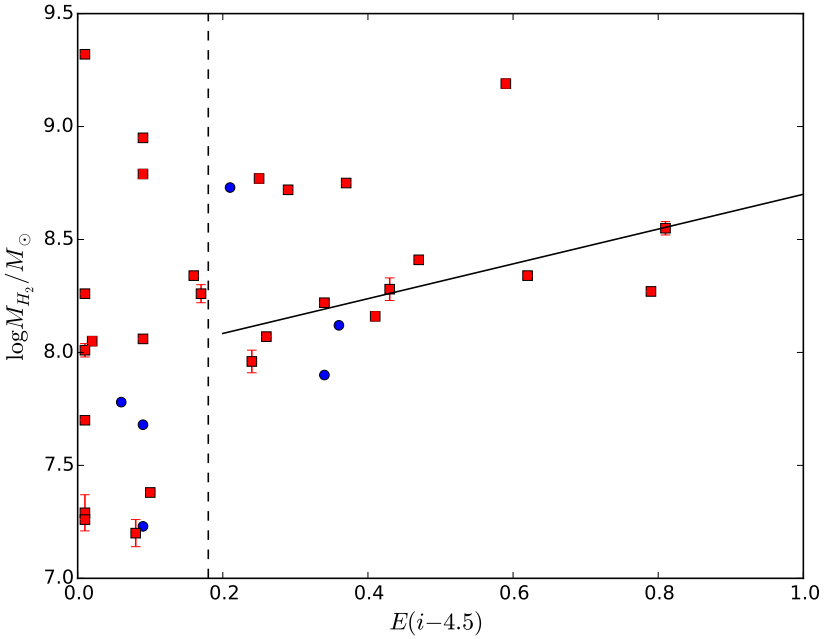

Figure 4.2: CO mass versus $(i - 4.5)$ colour excess of dust in S0 galaxies. Lower limit detections are shown with blue solid circles.

However, to improve the trend that we see in Figure 4.1 and 4.2, we need to (1) study large sample of early-type galaxies with optical-IR colour map and corresponding CO M_{H_2} measurement (2) improve optical-IR colour excess by employing various method and reduce error in these measurements.

Chapter 5

Conclusion

In this thesis, we made use of data available from Spitzer Space Telescope and Sloan Digital Sky Survey (SDSS) to study the dust and associated with molecular gas properties of a sample of S0 galaxies. A variety of image processing techniques were employed to study the details of galaxies to uncover the presence of molecular gas in S0 galaxies including optical-IR colour maps using 3.6 (or 4.5) micron images and SDSS r (or i) band images. Below we summarize few important results:

- These galaxies have sufficient amount of dust and molecular gas along with variety of dust morphologies.
- A half (50%) of the sample had disturbed dust, ∼11% dust ring, ∼5% spiral dust, ∼17% dust lanes, and ∼17% transition case between ring and non-ring dust. These morphologies suggest that these galaxies had minor mergers in the recent past to have the amount of dust and gas detected.
- We have shown, for the first time that the mass of molecular gas obtained by CO is correlated to colour excess measured from $(r - 3.6)$ colour maps indicating that optical-IR colour excess is a reliable tracer of the dense molecular gas. It would be important to study this relation using advance facilities such as ALMA (Atacama Large Millimeter/Submillimeter Array) and MeerKAT (Karoo Array Telescope) to explore properties of molecular gas in nearby early-type galaxies in detail.

In future, we plan to extend this work to derive colour excess more accurately using various methods describe in literature using colour and dust extinction maps that can be converted to approximate dust mass maps based on dust geometries. We would like to employ different methods to determine the colour excess hence the total dust mass in the dust lane. For example, we would like to use following methods:

- SED fitting from Optical to FIR/sub-mm observations using code like *MAGPHYS*.

- Multi-Gaussian Expansion (MGE) fitting to obtain dust free model which can be compare with observed galaxy image to construct monochromatic dust extinction maps in each waveband.
- Radiative transfer modeling. This is the advanced way to measure dust extinction through radiative transfer (RT) simulations using FitSKIRT (De Geyter et al. 2013, De Geyter & Baes 2014) code.

These methods would not only help us to derive colour excess more accurately but also various parameters like dust mass, host galaxy mass, age, star formation rate and etc. These parameters along with molecular gas mass, neutral hydrogen (HI) mass would be use to study processes responsible for presence of dust and molecular gas. This in turn will allows us to investigate galaxy formation process and their effect on various galaxy properties.

Bibliography

Abadi, M. G., Moore, B., & Bower, R. G. 1999, MNRAS, 308, 947

Aguerri, J. A. L., Gerhard, O. E., Arnaboldi, M., Napolitano, N. R., Castro-Rodriguez, N., & Freeman, K. C. 2005, AJ, 129, 2585

Alatalo, K., Crocker, A. F., Aalto, S., Davis, T. A., Nyland, K., Bureau, M., Duc, P.-A., Krajnović, D., & Young, L. M. 2015, MNRAS, 450, 3874

Allamandola, L. J., Hudgins, D. M., Bauschlicher, Jr., C. W., & Langhoff, S. R. 1999, A&A, 352, 659

Allen, T. S., Prchlik, J. J., Megeath, S. T., Gutermuth, R. A., Pipher, J. L., Naylor, T., & Jeffries, R. D. 2014, The Astrophysical Journal, 786, 113

Aragón-Salamanca, A., Bedregal, A. G., & Merrifield, M. R. 2006, A&A, 458, 101

Baldry, I. K., Glazebrook, K., Brinkmann, J., Ivezić, Ž., Lupton, R. H., Nichol, R. C., & Szalay, A. S. 2004, ApJ, 600, 681

Barr, J. M., Bedregal, A. G., Aragón-Salamanca, A., Merrifield, M. R., & Bamford, S. P. 2007, A&A, 470, 173

Barway, S., Kembhavi, A., Wadadekar, Y., Ravikumar, C., & Mayya, Y. 2007, The Astrophysical Journal Letters, 661, L37

Barway, S., Wadadekar, Y., & Kembhavi, A. K. 2011, Monthly Notices of the Royal Astronomical Society: Letters, 410, L18

Barway, S., Wadadekar, Y., Kembhavi, A. K., & Mayya, Y. 2009, Monthly Notices of the Royal Astronomical Society, 394, 1991

Barway, S., Wadadekar, Y., Vaghmare, K., & Kembhavi, A. K. 2013, Monthly Notices of the Royal Astronomical Society, 432, 430

Bedregal, A. G., Aragón-Salamanca, A., & Merrifield, M. R. 2006, MNRAS, 373, 1125

Bekki, K. 1998, ApJ, 502, L133

Binney, J. & Merrifield, M. 1998, Galactic Astronomy

Bohlin, R. C., Savage, B. D., & Drake, J. 1978, The Astrophysical Journal, 224, 132

Boselli, A., Casoli, F., & Lequeux, J. 1995, Astronomy and Astrophysics Supplement Series, 110, 521

Braine, J. & Combes, F. 1992, Astronomy and Astrophysics, 264, 433

Cappellari, M., Emsellem, E., Krajnović, D., McDermid, R. M., Scott, N., Kleijn, G. V., Young, L. M., Alatalo, K., Bacon, R., Blitz, L., et al. 2011, Monthly Notices of the Royal Astronomical Society, 413, 813

Constantin, A., Hoyle, F., & Vogeley, M. S. 2008, ApJ, 673, 715

Côté, P., Piatek, S., Ferrarese, L., Jordán, A., Merritt, D., Peng, E. W., Haşegan, M., Blakeslee, J. P., Mei, S., West, M. J., et al. 2006, The Astrophysical Journal Supplement Series, 165, 57

Crocker, A. F., Bureau, M., Young, L. M., & Combes, F. 2011, MNRAS, 410, 1197

da Cunha, E., Charlot, S., & Elbaz, D. 2008, MNRAS, 388, 1595

Davis, T. A., Greene, J., Ma, C.-P., Pandya, V., Blakeslee, J. P., McConnell, N., & Thomas, J. 2015, ArXiv e-prints

De Geyter, G. & Baes, M. 2014, in Astronomical Society of the Pacific Conference Series, Vol. 480, Structure and Dynamics of Disk Galaxies, ed. M. S. Seigar & P. Treuthardt, 243

De Geyter, G., Baes, M., Fritz, J., & Camps, P. 2013, A&A, 550, A74

Driver, S. P., Allen, P. D., Graham, A. W., Cameron, E., Liske, J., Ellis, S. C., Cross, N. J. G., De Propris, R., Phillipps, S., & Couch, W. J. 2006, MNRAS, 368, 414

Ebneter, K., Davis, M., & Djorgovski, S. 1988, AJ, 95, 422

Faber, S. M., Willmer, C. N. A., Wolf, C., Koo, D. C., Weiner, B. J., Newman, J. A., Im, M., Coil, A. L., Conroy, C., Cooper, M. C., Davis, M., Finkbeiner, D. P., Gerke, B. F., Gebhardt, K., Groth, E. J., Guhathakurta, P., Harker, J., Kaiser, N., Kassin, S., Kleinheinrich, M., Konidaris, N. P., Kron, R. G., Lin, L., Luppino, G., Madgwick, D. S., Meisenheimer, K., Noeske, K. G., Phillips, A. C., Sarajedini, V. L., Schiavon, R. P., Simard, L., Szalay, A. S., Vogt, N. P., & Yan, R. 2007, ApJ, 665, 265

Fazio, G. G., Hora, J. L., Allen, L. E., Ashby, M. L. N., Barmby, P., Deutsch, L. K., Huang, J.-S., Kleiner, S., Marengo, M., Megeath, S. T., Melnick, G. J., Pahre, M. A., Patten, B. M., Polizotti, J., Smith, H. A., Taylor, R. S., Wang, Z., Willner, S. P., Hoffmann, W. F., Pipher, J. L., Forrest, W. J., McMurty, C. W., McCreight, C. R., McKelvey, M. E., McMurray, R. E., Koch, D. G., Moseley, S. H., Arendt, R. G., Mentzell, J. E., Marx, C. T., Losch, P., Mayman, P., Eichhorn, W., Krebs, D., Jhabvala, M., Gezari, D. Y., Fixsen, D. J., Flores, J., Shakoorzadeh, K., Jungo, R., Hakun, C., Workman, L.,

Karpati, G., Kichak, R., Whitley, R., Mann, S., Tollestrup, E. V., Eisenhardt, P., Stern, D., Gorjian, V., Bhattacharya, B., Carey, S., Nelson, B. O., Glaccum, W. J., Lacy, M., Lowrance, P. J., Laine, S., Reach, W. T., Stauffer, J. A., Surace, J. A., Wilson, G., Wright, E. L., Hoffman, A., Domingo, G., & Cohen, M. 2004, ApJS, 154, 10

Gadotti, D. A. 2009, MNRAS, 393, 1531

Gehrz, R., Roellig, T., Werner, M., Fazio, G., Houck, J., Low, F., Rieke, G., Soifer, B., Levine, D., & Romana, E. 2007, Review of scientific instruments, 78, 011302

Goudfrooij, P., Hansen, L., Jorgensen, H. E., Norgaard-Nielsen, H. U., de Jong, T., & van den Hoek, L. B. 1994, A&AS, 104, 179

Guélin, M., Zylka, R., Mezger, P., Haslam, C., Kreysa, E., Lemke, R., & Sievers, A. 1993, Astronomy and Astrophysics, 279, L37

Houck, J., Roellig, T., Van Cleve, J., Forrest, W., Herter, T., Lawrence, C., Matthews, K., Reitsema, H., Soifer, B., Watson, D., et al. 2004, The Astrophysical Journal Supplement Series, 154, 18

Hubble, E. P. 1936, The realm of the nebulae (Yale University Press)

Israel, F. 2000, in Molecular Hydrogen in Space, ed. F. Combes & G. Pineau Des Forets, 293

Joye, W. A. & Mandel, E. 2003, in Astronomical Society of the Pacific Conference Series, Vol. 295, Astronomical Data Analysis Software and Systems XII, ed. H. E. Payne, R. I. Jedrzejewski, & R. N. Hook, 489

Kaviraj, S., Crockett, R. M., Silk, J., Ellis, R. S., Yi, S. K., O'Connell, R. W., Windhorst, R., & Whitmore, B. C. 2012, in IAU Symposium, Vol. 284, IAU Symposium, ed. R. J. Tuffs & C. C. Popescu, 460–464

Kent, S. M. 1994, in Science with Astronomical Near-Infrared Sky Surveys (Springer), 27–30

Knapen, J. H., Erroz-Ferrer, S., Roa, J., Bakos, J., Cisternas, M., Leaman, R., & Szymanek, N. 2014, A&A, 569, A91

Knapp, G. R. 1999, in Astronomical Society of the Pacific Conference Series, Vol. 163, Star Formation in Early Type Galaxies, ed. P. Carral & J. Cepa, 119

Kormendy, J. & Bender, R. 1996, The Astrophysical Journal Letters, 464, L119

Kormendy, J. & Kennicutt, Jr., R. C. 2004, ARA&A, 42, 603

Kulkarni, S., Sahu, D., Chaware, L., Chakradhari, N., & Pandey, S. 2014, New Astronomy, 30, 51

Lagos, C. d. P., Padilla, N. D., Davis, T. A., Lacey, C. G., Baugh, C. M., Gonzalez-Perez, V., Zwaan, M. A., & Contreras, S. 2015, MNRAS, 448, 1271

Li, J. G., Seaquist, E. R., Wrobel, J. M., Wang, Z., & Sage, L. J. 1993, ApJ, 413, 150

Liszt, H. S. 2007, A&A, 476, 291

Liszt, H. S., Pety, J., & Lucas, R. 2010, A&A, 518, A45

Makarov, D., Prugniel, P., Terekhova, N., Courtois, H., & Vauglin, I. 2014, A&A, 570, A13

McDermid, R. M., Alatalo, K., Blitz, L., Bournaud, F., Bureau, M., Cappellari, M., Crocker, A. F., Davies, R. L., Davis, T. A., de Zeeuw, P. T., Duc, P.-A., Emsellem, E., Khochfar, S., Krajnović, D., Kuntschner, H., Morganti, R., Naab, T., Oosterloo, T., Sarzi, M., Scott, N., Serra, P., Weijmans, A.-M., & Young, L. M. 2015, MNRAS, 448, 3484

Naab, T., Jesseit, R., & Burkert, A. 2006, MNRAS, 372, 839

Neininger, N., Guelin, M., Garcia-Burillo, S., Zylka, R., & Wielebinski, R. 1996, Astronomy and Astrophysics, 310, 725

Padmanabhan, N., Schlegel, D. J., Finkbeiner, D. P., Barentine, J. C., Blanton, M. R., Brewington, H. J., Gunn, J. E., Harvanek, M., Hogg, D. W., Ivezić, Ž., Johnston, D., Kent, S. M., Kleinman, S. J., Knapp, G. R., Krzesinski, J., Long, D., Neilsen, Jr., E. H., Nitta, A., Loomis, C., Lupton, R. H., Roweis, S., Snedden, S. A., Strauss, M. A., & Tucker, D. L. 2008, ApJ, 674, 1217

Patil, M. K., Pandey, S. K., Sahu, D. K., & Kembhavi, A. 2007, A&A, 461, 103

Paturel, G., Petit, C., Prugniel, P., Theureau, G., Rousseau, J., Brouty, M., Dubois, P., & Cambresy, L. 2003, VizieR Online Data Catalog, 7237, 0

Pirronello, V., Manicó, G., Roser, J., & Vidali, G. 2004, in Astrophysics of dust, Vol. 309, 529

Pogge, R. W. & Martini, P. 2002, ApJ, 569, 624

Pota, V., Forbes, D. A., Romanowsky, A. J., Brodie, J. P., Spitler, L. R., Strader, J., Foster, C., Arnold, J. A., Benson, A., Blom, C., et al. 2012, Monthly Notices of the Royal Astronomical Society

Rahman, N., Bolatto, A. D., Wong, T., Leroy, A. K., Walter, F., Rosolowsky, E., West, A. A., Bigiel, F., Ott, J., Xue, R., et al. 2011, The Astrophysical Journal, 730, 72

Rieke, G., Young, E., Engelbracht, C., Kelly, D., Low, F., Haller, E., Beeman, J., Gordon, K., Stansberry, J., Misselt, K., et al. 2004, The Astrophysical Journal Supplement Series, 154, 25

Rubio, M., Lequeux, J., Boulanger, F., Booth, R. S., Garay, G., de Graauw, T., Israel, F. P., Johansson, L. E. B., Kutner, M. L., & Nyman, L. A. 1993, A&A, 271, 1

Sadler, E. M. 1985, in Cosmical Gas Dynamics, ed. F. D. Kahn, 27–32

Salim, S., Rich, R. M., Charlot, S., Brinchmann, J., Johnson, B. D., Schiminovich, D., Seibert, M., Mallery, R., Heckman, T. M., Forster, K., Friedman, P. G., Martin, D. C., Morrissey, P., Neff, S. G., Small, T., Wyder, T. K., Bianchi, L., Donas, J., Lee, Y.-W., Madore, B. F., Milliard, B., Szalay, A. S., Welsh, B. Y., & Yi, S. K. 2007, ApJS, 173, 267

Sánchez-Janssen, R. & Aguerri, J. A. L. 2012, MNRAS, 424, 2614

Schawinski, K., Lintott, C. J., Thomas, D., Kaviraj, S., Viti, S., Silk, J., Maraston, C., Sarzi, M., Yi, S. K., Joo, S.-J., Daddi, E., Bayet, E., Bell, T., & Zuntz, J. 2009, ApJ, 690, 1672

Schawinski, K., Thomas, D., Sarzi, M., Maraston, C., Kaviraj, S., Joo, S.-J., Yi, S. K., & Silk, J. 2007, MNRAS, 382, 1415

Sheth, K., Regan, M., Hinz, J. L., de Paz, A. G., Menéndez-Delmestre, K., Muñoz-Mateos, J.-C., Seibert, M., Kim, T., Laurikainen, E., Salo, H., et al. 2010, Publications of the Astronomical Society of the Pacific, 122, 1397

Sheth, K., Regan, M. W., Thornley, M. D., Blitz, L., Bock, D. C.-J., Harris, A., Helfer, T. T., Vogel, S. N., & Wong, T. 1998, in Bulletin of the American Astronomical Society, Vol. 30, American Astronomical Society Meeting Abstracts, 1354

Sheth, K., Regan, M. W., Vogel, S. N., & Teuben, P. J. 2000, The Astrophysical Journal, 532, 221

Sheth, K., Regan, M. W., Vogel, S. N., & Teuben, P. J. 2000, ApJ, 532, 221

Sheth, K., Vogel, S. N., Regan, M. W., Teuben, P. J., Harris, A. I., & Thornley, M. D. 2002, The Astronomical Journal, 124, 2581

Skibba, R. A., Masters, K. L., Nichol, R. C., Zehavi, I., Hoyle, B., Edmondson, E. M., Bamford, S. P., Cardamone, C. N., Keel, W. C., Lintott, C., & Schawinski, K. 2012, MNRAS, 423, 1485

Smith, M., Gomez, H., Eales, S., Ciesla, L., Boselli, A., Cortese, L., Bendo, G., Baes, M., Bianchi, S., Clemens, M., et al. 2012, The Astrophysical Journal, 748, 123

Solomon, P. M., Downes, D., Radford, S. J. E., & Barrett, J. W. 1997, ApJ, 478, 144

Solomon, P. M., Rivolo, A. R., Barrett, J., & Yahil, A. 1987, ApJ, 319, 730

Thronson Jr, H. A., Tacconi, L., Kenney, J., Greenhouse, M. A., Margulis, M., Tacconi-Garman, L., & Young, J. S. 1989, The Astrophysical Journal, 344, 747

Tody, D. 1986, in Society of Photo-Optical Instrumentation Engineers (SPIE) Conference Series, Vol. 627, Instrumentation in astronomy VI, ed. D. L. Crawford, 733

van den Bergh, S. 2012, ApJ, 754, 68

Wei, L. H., Vogel, S. N., Kannappan, S. J., Baker, A. J., Stark, D. V., & Laine, S. 2010, The Astrophysical Journal Letters, 725, L62

Wiklind, T. & Henkel, C. 1989, Astronomy and Astrophysics, 225, 1

Wilson, C. D., Walker, C. E., & Thornley, M. D. 1995, in Bulletin of the American Astronomical Society, Vol. 27, American Astronomical Society Meeting Abstracts, 1375

York, D. G., Adelman, J., Anderson Jr, J. E., Anderson, S. F., Annis, J., Bahcall, N. A., Bakken, J., Barkhouser, R., Bastian, S., Berman, E., et al. 2000, The Astronomical Journal, 120, 1579

Young, L. M., Bureau, M., Davis, T. A., Combes, F., McDermid, R. M., Alatalo, K., Blitz, L., Bois, M., Bournaud, F., Cappellari, M., et al. 2011, Monthly Notices of the Royal Astronomical Society, 414, 940